
A human lung organoid platform for studying radiation-induced pulmonary fibrosis and antifibrotic drug screening

Received: 7 July 2025

Accepted: 3 December 2025

Published online: 29 December 2025

Cite this article as: Park H., Kwon Y., Ji H.J. *et al.* A human lung organoid platform for studying radiation-induced pulmonary fibrosis and antifibrotic drug screening. *Sci Rep* (2025). <https://doi.org/10.1038/s41598-025-31582-1>

Hae-Ran Park, Yeongkag Kwon, Hyun Jung Ji, Sun-Young Kim, Min-Kyu Kim, Ki Bum Ahn & Ho Seong Seo

We are providing an unedited version of this manuscript to give early access to its findings. Before final publication, the manuscript will undergo further editing. Please note there may be errors present which affect the content, and all legal disclaimers apply.

If this paper is publishing under a Transparent Peer Review model then Peer Review reports will publish with the final article.

A Human Lung Organoid Platform for Studying Radiation-Induced Pulmonary Fibrosis and Antifibrotic Drug Screening

Hae-Ran Park^{1,†*}, Yeongkag Kwon^{1,†}, Hyun Jung Ji¹, Sun-Young Kim^{1,2}, Min-Kyu Kim¹, Ki Bum Ahn¹, Ho Seong Seo^{1,3*}

¹Cyclotron Applied Research Section, Advanced Radiation Technology Institute, Korea Atomic Energy Research Institute (KAERI), Jeongeup 56212, Republic of Korea

²School of Biological Sciences and Institute of Microbiology, Seoul National University, Seoul, 08826, Republic of Korea

³Department of Radiation Science, University of Science and Technology, Daejeon, Republic of Korea

*Correspondence to: Ho Seong Seo and Hae-Ran Park, Advanced Radiation Technology Institute, Korea Atomic Energy Research Institute (KAERI), 29 Geumgu-gil, Jeongeup-si, Jeollabuk-do 56212, Republic of Korea. Tel.: 82-63-570-3221, Fax: 82-63-570-3229, e-mail: hoseongseo@kaeri.re.kr

†Hae-Ran Park and Yeongkag Kwon contributed equally to this work; author order was determined in order of increasing seniority.

Keywords: Ionizing radiation, Embryonic stem cell, Lung organoid, Fibrosis, epithelial to mesenchymal transition

Running title: Lung Organoid Model for RIPF and Drug Screening

ABSTRACT

Radiation-induced pulmonary injury and fibrosis (RIPI/RIPF) is a major complication following thoracic radiotherapy, characterized by persistent inflammation and excessive extracellular matrix deposition leading to irreversible lung disease. The development of antifibrotic drugs has been limited by the lack of physiologically relevant *in vitro* models that mimic the complex lung microenvironment. In this study, we established a human embryonic stem cells-derived human lung organoids (hLOs) model, comprising major epithelial cell types, including AT1, AT2, goblet, basal, club, and ciliated cells. Following repeated irradiation, hLOs exhibited key features of RIPF, including impaired proliferation, epithelial barrier disruption, epithelial-mesenchymal transition, upregulation of profibrotic cytokines, and extensive collagen deposition. Single-cell RNA sequencing revealed a marked reduction in proliferative AT2 cells and shifts in epithelial subpopulations, mimicking cellular dynamics observed *in vivo*. Importantly, Pirfenidone, an antifibrotic drug, significantly reduced the expression of TGF- β , α -SMA, and COL1A2 in irradiated hLOs. These findings demonstrate that our hESC-derived hLO model recapitulates key molecular and structural features of RIPF and offers a human-relevant, scalable platform for mechanistic studies and antifibrotic drug screening. This organoid system provides a time-efficient alternative to conventional animal models, enabling fibrosis-like responses, and may serve as a valuable tool for advancing therapeutic strategies against RIPI/RIPF.

INTRODUCTION

Radiation-induced pulmonary injury (RIPI) progresses through distinct stages, beginning with acute pneumonitis and culminating in late-stage pulmonary fibrosis^{1,2}. During the early phase, radiation pneumonitis is characterized by epithelial and endothelial cell damage, infiltration of inflammatory cells, and the release of proinflammatory cytokines such as IL-1 β , TNF- α , and TGF- β . These events promote fibroblast activation, extracellular matrix (ECM) deposition, and collagen synthesis in the late stage^{3,4}. Pulmonary fibrosis, the chronic and often irreversible consequence of RIPI, affects approximately 5-50% of patients receiving thoracic radiotherapy for lung or breast cancers^{5,6}. Despite improvements in radiotherapy techniques to minimize off-target toxicity and improve precisely tumor targeting, the risk of radiation-induced pulmonary injury (RIPF) remains clinically significant⁷.

Current treatments strategies, including myofibroblast differentiation inhibition (e.g., Pirfenidone, PFD), blockade of non-Smad pathways (e.g., thalidomide), corticosteroids (e.g., prednisone), immunosuppressants (e.g., azathioprine), and angiotensin-converting enzyme (ACE) inhibitors, primarily focus on managing symptoms or slowing disease progression^{8,9}. However, these therapies are insufficient to cease or reverse established fibrosis, highlighting an urgent need for novel antifibrotic drugs and more effective disease management approaches⁹. One of the key obstacles to developing antifibrotic drugs is the lack of physiologically relevant *in vitro* models that replicate the complexity of human alveolar architecture and the underlying pathophysiology of RIPF^{10,11}.

Traditionally, immortalized lung epithelial cancer cell lines, such as A549, have been widely used to study the molecular mechanism and facilitate preliminary drug screening for RIPF^{12,13}. Nevertheless, these cell lines are unable to replicate the structural complexity of the lung microenvironment and often exhibit altered genetic functional properties, limiting their relevance as accurate disease models^{14,15}. Animal models induced by irradiation or bleomycin have served as the standard tools for RIPF,

providing valuable insights into disease mechanisms and therapeutic targets¹⁶⁻¹⁸. However, these models are constrained by interspecies physiological differences and require prolonged durations (4-6 months) to fully develop fibrotic features, limiting their applicability for rapid and high-throughput drug screening¹⁸⁻²⁰. Recently, advanced *in vitro* models that more accurately replicate the human lung microenvironment have been developed, including lung alveolus-on-a-chip platforms and three-dimensional (3D) lung tissue models^{21,22}. Human lung-on-a-chip models combine human alveolar epithelial cells and pulmonary endothelial cells in microfluidic devices, enabling a platform to study early-stages RIPF features, such as DNA damage response, inflammation, collagen expression, and barrier dysfunction²¹. Similarly, 3D *in vitro* models, including precision-cut lung slices embedded in hydrogels, replicate the complex architecture and cellular diversity of the lung^{23,24}. However, lung slice models are difficult to produce in large quantities for drug screening, and lung-on-a-chip models struggle to mimic the diverse cellular composition of lung tissue, limiting their utility for RIPF drug development.

Organoids, which have recently been in the spotlight in various research fields, are 3D cellular structures derived from stem cells that can replicate the architecture and function of human organs^{25,26}. The development of lung organoids from human pluripotent stem cell (embryonic stem cells (ESC) or induced pluripotent stem cells (iPSC)) offers great promise for emulating native lung physiology and pathophysiology^{26,27}. Although organoid systems have not yet been extensively applied in RIPF drug discovery, they are emerging as a next-generation platform for radiobiological risk assessment and therapeutic discovery^{27,28}. ESC-derived organoids possess the most complete pluripotency due to their embryonic origin, offering advantages such as more mature, consistent, and stable differentiation efficiency compared to iPSC-derived organoids. However, ethical concerns and regulations impose significant constraints on their access and supply. iPSCs can be generated from a patient's somatic cells, offering the advantage of creating personalized disease

models. However, the reprogramming process carries the risk of genetic mutations or incomplete recombination, potentially resulting in immature organoids.

In this study, we employed human ESC-derived lung organoids (hLOs) to model radiation-induced lung fibrosis. We analyzed their growth characteristics, cellular composition, and fibrogenic marker expression following irradiation. Furthermore, we demonstrated the potential of this platform for antifibrotic drug screening by evaluating the therapeutic efficacy of Pirfenidone. Our findings support the use of hESC-derived lung organoids as a physiologically relevant and scalable *in vitro* model for RIPF and as a tool for the identification of novel therapeutic targets.

RESULTS

Development and Characterization of hLOs from hESCs

Human lung organoids (hLOs) were generated from hESCs using a previously established protocol²⁹. The differentiation process sequentially progressed through the definitive endoderm (DE) stage (Day 2), anterior foregut endoderm (AFE) stage (Day 8), ventral anterior foregut endoderm (VAFE) stage (Day 12), lung progenitor stage (Day 18), and finally into lung organoids (Day 33) (Figure 1A and Figure S1). The resulting hLOs exhibited stable phenotypes through at least ten passages, with passages 3 to 8 used for experimental analysis. To characterize the molecular diversity of the human lung, qRT-PCR and immunofluorescence staining were performed on passage 6 organoids. As shown in Figures 1B and 1C, hLOs exhibited strong expression of podoplanin (PDPN; alveolar type (AT) 1 marker), surfactant protein A1 (SFTPA1; AT2 marker), TP63 (basal cell marker), and Muc5Ac (goblet cell marker), supporting the presence of bronchioalveolar cell types. These results suggest that hLOs exhibits cellular heterogeneity, as it contains some human lung cells that constitute both alveolar and bronchial lineages.

Radiation Exposure Inhibits Growth and Proliferation of hLOs

To establish a fibrosis model, hLOs were irradiated with γ -rays at 2, 4, or 8 Gy on Day 1 and Day 3 (Figure 2A). Organoids exposed to two cycles of 4 Gy or higher displayed extensive cell death, whereas lower doses allowed partial survival. Therefore, we selected the 4 Gy \times 2 as an optimal irradiation condition for RIPF. Following two irradiation cycles, hLOs exhibited a significant reduction in growth and failed to regenerate (Figure 2B). Organoid size decreased in a dose-dependent manner after the first exposure and further declined after the second exposure, particularly under 4 Gy \times 2 and higher (Figure 2C). To quantify whether this size reduction was due to loss of proliferative capacity, we performed Ki-67 immunofluorescence staining (Figure 2D). Proliferative capacity was severely impaired, with fewer than five Ki-67⁺ cells per organoid compared

to ~30 in unirradiated controls (Figure 2E). These findings suggest that radiation induces apoptosis and suppresses proliferation of lung cells. Furthermore, the early loss of these proliferative epithelial cells is a hallmark of radiation-induced fibrotic progression, suggesting that this may be a pathological feature of RIPF.

Single-Cell Transcriptomic Analysis Reveals Cellular Reorganization in Irradiated hLOs

To elucidate the cellular dynamics and transcriptomic changes induced by radiation, we performed single-cell RNA sequencing (scRNA-seq) on dissociated human lung organoids (hLOs) from both control and irradiated groups (Figure 3A). A total of 17,155 cells were analyzed, including 10,265 cells from control hLOs and 6,890 cells from hLOs irradiated with 4 Gy × 2, representing a 32.9% reduction in total cell number following radiation exposure. Clustering and cell-type annotation revealed eight major epithelial subpopulations: alveolar type 1 (AT1) cells (7.6%), alveolar type 2 (AT2) cells (20.3%), proliferating AT2 cells (33.2%), goblet cells (12.2%), club cells (7.6%), basal cells (2.1%), ciliated cells (16.1%), and rare cell types (0.9%) (Figure 3B and 3C). These results confirm that the hLOs generated in this study reproduce the complex epithelial architecture of the human lung, encompassing both alveolar and airway lineages.

Upon irradiation, a notable reduction in proliferating AT2 cells was observed, reduction by 73.5% to comprise only 13.1% of the irradiated cell population, highlighting a key vulnerability of regenerative alveolar progenitors to radiation-induced damage. Interestingly, the relative proportions of several other cell types increased: ciliated cells by 59.6%, basal cells by 71.4%, AT1 cells by 26.3%, AT2 cells by 15.3%, goblet cells by 17.2%, and club cells by 14.5% (Figure 3B & C). Although basal cells accounted for only a small fraction of the total population, their increase was the most pronounced, suggesting a potential compensatory response to injury. Basal and AT2 cells are known to serve as progenitor populations capable of regenerating multiple epithelial cell types, including AT1 cells,

goblet cells, club cells, and ciliated cells, particularly during lung injury and repair^{25,30}.

Irradiated hLOs Exhibit EMT-like Changes and Abnormal differentiation

Epithelial-mesenchymal transition (EMT) plays a key mechanism in RIPF pathogenesis by converting epithelial cells into mesenchymal-like cells³¹. A key hallmark of EMT is the downregulation of E-cadherin and occludin, along with the upregulation of mesenchymal markers such as N-cadherin, vimentin, α -SMA, and collagen III³¹. To assess radiation-induced EMT in hLOs, we analyzed the expression patterns of key EMT-related markers after 4 Gy \times 2 exposure using western blot analysis and qRT-PCR. Irradiated hLOs exhibited upregulation of N-cadherin, vimentin, α -SMA, and collagen III, along with downregulation of E-cadherin and occludin (Figure 4A and Figure S4). These findings were correlated by immunofluorescence imaging (Figure 4B).

Among these EMT markers, α -SMA exhibited the most dramatic upregulation after repeated irradiation. As shown in Figure 4C, α -SMA mRNA was nearly undetectable in unirradiated or a single 4 Gy irradiated hLOs, but its expression markedly increased after the second 4 Gy irradiation. Immunofluorescence staining also revealed strong α -SMA expression in irradiated hLOs (Figure 4D). Furthermore, we confirmed that all epithelial cell subpopulations in irradiated hLOs showed high ACTA2 (α -SMA) expression (Figure S2). These results indicate that radiation induces EMT-like phenotypes in hLOs, promoting epithelial barrier dysfunction, senescence, and aberrant differentiation.

Ionizing Radiation Induces Collagen expression *in vivo* and in hLO

Pulmonary fibrosis following thoracic irradiation is characterized by excessive deposition of collagen isoforms, which disrupts the normal alveolar architecture and impairs lung function³². To evaluate an *in vivo* model of RIPF, mice were exposed to a single dose of 14 Gy thoracic irradiation (Figure 5A). Histopathological analysis was performed at 4- and

6-months post-irradiation, which are well-established time points in previous studies for evaluating late-onset radiation-induced lung fibrosis following a 14 Gy thoracic dose^{18,19}. Compared to the control group, the irradiated mice exhibited significantly increased inflammation scores in the vascular, airway, and parenchymal compartments of the lung (Figure 5B-E). In addition, Masson's trichrome staining revealed marked collagen accumulation in the peribronchial regions and alveolar interstitium of irradiated lungs, confirming the development of fibrosis (Figure 5B and F).

Based on the histopathological and molecular characteristics observed in the *in vivo* RIPF mouse model, we next investigated whether irradiated hLOs exhibit comparable fibrotic features. qRT-PCR analysis revealed a significant upregulation of fibrotic markers COL1A1, COL1A2, and COL3A1 in irradiated hLOs, with COL1A2 showing the most pronounced increase (Figure 5G-I). These transcriptional changes were further supported by immunofluorescence staining, which demonstrated robust accumulation of type I and type III collagen proteins, particularly in the inter-epithelial regions (Figure 5J and K). These findings indicate that irradiated hLOs undergo fibrotic remodeling characterized by excessive collagen deposition, mimicking the pathological features observed in the *in vivo* RIPF model. This result demonstrates the potential of hLOs as a physiologically relevant *in vitro* platform for studying radiation-induced pulmonary fibrosis.

Ionizing radiation induces profibrotic cytokine *in vivo* and in hLO

Among various profibrotic cytokines, growth factors such as TGF-β, GDF-15, and PDGF play key roles in stimulating fibroblasts and epithelial cells, thereby promoting ECM remodeling and contributing to ultimately induce pulmonary fibrosis³³⁻³⁷. To confirm whether these factors are involved in our *in vivo* model of radiation-induced lung fibrosis, we measured TGF-β levels in bronchoalveolar lavage (BAL) fluid and GDF-15 expression in lung tissues of thoracically irradiated mice (Figure 6A and B). Both TGF-β and GDF-15 levels were significantly elevated at 4- and 6-months post-

irradiation, supporting their roles as key mediators of fibrosis in this model.

To evaluate the fibrotic response of hLOs to radiation, we measured the expression of key profibrotic cytokines and compared these results to the *in vivo* RIPF model. qRT-PCR analysis revealed that the mRNA levels of TGF- β , GDF-15, and PDGF-A were markedly increased after repeated irradiation (Figure 6C-E). Notably, TGF- β mRNA expression was not significantly elevated after a single irradiation, even at higher doses. However, sequential exposure to 4 Gy administered twice resulted in a significant upregulation of TGF- β . Similarly, GDF-15 and PDGF-A mRNA levels were significantly increased only after repeated irradiation, suggesting that cumulative radiation exposure is critical for inducing a fibrotic gene expression program in hLOs. We identified which epithelial cells primarily secrete these key pro-fibrotic cytokines by scRNAseq analysis. As a result, GDF15 expression was shown to be significantly increased in all epithelial cells constituting bronchi and alveoli compared to unirradiated hLOs (Figure S2C). TGF- β and PDGF-A were confirmed to have increased expression in specific cells, although the expression amounts were low: TGF- β was expressed by both AT1 and AT2 cells that constitute the alveoli and was also expressed in goblet cells among cells that constitute the bronchi (Figure S2B), and PDGF was confirmed to be expressed in AT2 cells and club cells (Figure S2D). These results demonstrate that irradiated hLOs exhibited transcriptional and structural changes that closely mimic those observed *in vivo* pulmonary fibrosis model. These fibrosis-like phenotypes in hLOs developed as early as 4 to 7 days following irradiation, providing a significant experimental time advantage over conventional mice models, which typically require several months to develop comparable pathological features.

Effect of Pirfenidone on hLO model of RIPI/RIPF

To validate the utility of hLO as a screening platform for RIPI/RIPF, we tested the antifibrotic effects of PFD, an FDA-approved antifibrotic agent clinically used for idiopathic pulmonary fibrosis treatment^{38,39}. hLOs were

treated with PFD immediately following the first and second irradiation (Figure 7A). Compared to untreated controls, PFD significantly suppressed the expression of TGF- β , α -SMA, and COL1A2 (Figures 7B-D). These results confirm that hESC-derived lung organoids are suitable for antifibrotic drug screening and mechanistic studies of RIPF.

ARTICLE IN PRESS

DISCUSSTION

In this study, we established an *in vitro* human model using hESC-derived lung organoids (hLOs) to investigate radiation-induced pulmonary injury and fibrosis (RIPI/RIPF) and to evaluate antifibrotic drug screening. RIPI/RIPF remains a major clinical complication among thoracic cancer patients undergoing radiotherapy, yet its pathogenesis is not fully understood due to the limited availability of human-relevant *in vitro* models^{10,11}. Traditional animal models have been indispensable for studying RIPF, but significant physiological differences from humans, along with their long latency periods (typically 4–6 months), limit their use in efficient drug development and mechanistic studies. Similarly, immortalized lung epithelial cell lines fail to mimic the complex epithelial architecture and microenvironment of the human lung^{12–15}. Our hLOs, generated from hESCs, consist of multiple lung epithelial cell types including AT1, AT2, goblet, basal, club, and ciliated cells, and stably replicate key structural characteristics of the human lung. Notably, our model achieved rapid induction of fibrotic features within 4–7 days using a 4 Gy × 2 radiation exposure, compared to months required in animal models.

In our organoid model, we observed that radiation exposure resulted in hallmark features of RIPF, including growth arrest, apoptosis, cellular senescence, and epithelial barrier disruption. First, apoptosis and senescence are early and critical steps in fibrosis development and are typically accompanied by DNA damage response (DDR) activation post-irradiation^{40,41}. The DDR is regulated by the tumor suppressor protein p53⁴², which was markedly upregulated across all cell populations in our hLO fibrosis model (Figure S3). Second, lung tissue damage led to epithelial barrier disruption, characterized by the downregulation of tight and gap junction proteins. This disruption increases barrier permeability, allowing irritants, cytokine expression, and immune cell infiltration, which in turn triggers epithelial and fibroblast differentiation abnormalities⁴³. These changes were accompanied by molecular evidence of EMT, such as

upregulation of mesenchymal markers (N-cadherin, vimentin, α -SMA, and collagen III) and downregulation of epithelial junctional proteins (E-cadherin and occludin). EMT has been widely recognized as a key mechanism driving fibrogenesis and tissue remodeling following lung injury⁴¹. Our data suggests that radiation-induced disruption of epithelial integrity, rather than morphological changes alone, initiates the fibrotic cascade. The significant reduction in Ki-67⁺ cells and epithelial barrier proteins supports this result and suggests that growth retardation and epithelial dysfunction precede mesenchymal transition in this system.

During lung homeostasis and repair in the damaged lung, basal cells and AT2 cells serve as key stem cells populations, replacing injured and abnormal bronchial or alveolar epithelial cells³⁰. Upon radiation exposure, AT2 cells is reported to undergo EMT *via* ERK/GSK2 β /Snail signaling pathway, contributing to fibrosis development^{40,44}. Upon the destruction of AT1 cells, AT2 cells undergo an increase in proliferation and differentiate into AT1 cells, thereby facilitating the restoration of the alveolar epithelium. In addition, when cells in lung bronchus are destroyed, they are restored by differentiating and proliferating from basal cells into bronchial constituent cells. In our organoid model, we observed a significant decrease in the number and proportion of proliferative AT2 cells after radiation exposure, which is consistent with both mouse models and previous reported clinical data^{40,45-47}. In contrast, the number of basal cells were not reduced by irradiation, reflecting that AT2 cells are highly sensitive to radiation but basal cells are resistant. To overcome this limitation, future studies incorporating time-course scRNA-seq analyses will be essential for identifying dynamic gene expression changes and further elucidating the molecular mechanisms underlying RIPI and RIPF.

Recent evidence suggests that lung inflammatory signals following irradiation play a critical role in not only lung fibrosis, but alveolar regeneration^{31,48}. Immune cells release cytokines that stimulate fibroblasts and progenitor cells to differentiate into myofibroblast, promoting fibrosis and pulmonary macrophages are involved in damaging,

repairing and fibrosing the lung^{31,48}. Our previous study demonstrated increased expression of CCL2 and macrophage influx in the lungs following thoracic irradiation and the macrophages infiltration into the lungs were responsible for inducing EMT leading to fibrosis^{33,49}. Due to their pivotal role, co-culture techniques involving macrophages and hLOs have been explored to investigate the mechanisms of various lung diseases^{50,51}. However, a key limitation of hLOs fibrosis model used in this study is that RIPF development was observed without immune cells, such as macrophages. In fact, TGF- β levels, a major fibrosis-driving factor, are only modestly elevated (~2-fold) in irradiated hLOs, likely due to the absence of macrophages. Despite this limitation, our hLOs fibrosis model might be valuable *in vitro* model for RIPF, as it exhibits high expression of other fibrotic mediators, such as PDGF and GDF15, as well as substantial ECM component production. These findings highlight the potential of hLOs in studying RIPF pathogenesis and drug development. Furthermore, we successfully tested the antifibrotic effects of pirfenidone (PFD) using our hLO fibrosis model by measuring the expression of lung fibrosis markers, demonstrating its applicability in evaluating potential therapeutic interventions.

In summary, this study presents a robust, scalable, and human-relevant organoid-based platform for modeling RIPF that can recapitulate key pathological features within a short time frame. Ionizing radiation initiates epithelial damage in hLOs, resulting in impaired proliferation and loss of epithelial integrity. Furthermore, the damaged epithelium secretes profibrotic cytokines such as TGF- β , GDF-15, and PDGF-A, promoting aberrant differentiation of epithelial cells by EMT, which in turn promotes activation and deposition of ECM including type I and III collagens (Figure 8). Future efforts will focus on enhancing the cellular complexity of this model by including immune and stromal components and performing longitudinal transcriptomic analyses. We are confident that these refinements will further improve their value in mechanistic studies and translational drug development for radiation-induced lung diseases.

ARTICLE IN PRESS

MATERIALS AND METHODS

Chemicals, Antibodies, and Reagents

Human embryonic stem cells (hESCs; H9) and reagents for organoid culture were obtained from Organoid Sciences (Pangyo, Republic of Korea) and STEMCELL Technologies (Vancouver, Canada). Matrigel and Accutase were purchased from Corning Inc. (Corning, NY, USA) and Innovative Cell Technologies (San Diego, CA, USA), respectively. Pirfenidone was acquired from Sigma-Aldrich (St. Louis, MO, USA). Primary antibodies against collagen III, occludin, α -SMA, and Ki-67 were sourced from Invitrogen (Carlsbad, CA, USA), while antibodies for E-cadherin, N-cadherin, and collagen I were obtained from Cell Signaling Technology (Beverly, MA, USA). Antibodies specific for AT1 cells, AT2 cells, and β -actin were purchased from Santa Cruz Biotechnology (Santa Cruz, CA, USA). HRP-conjugated secondary antibodies and Alexa Fluor 488/568-conjugated antibodies were obtained from Cell Signaling Technology and Invitrogen, respectively. Alexa Fluor 488-phalloidin and 4',6-diamidino-2-phenylindole (DAPI) were also from Invitrogen.

The generation of Human ESC-derived Lung Organoid

The generation of hLOs) from hESCs (H9) was performed according to a previously established protocol²⁹. Briefly, to differentiate into definitive endoderm cells, the hESCs (H9) were plated on a Matrigel-coated 6-well plate at 8×10^5 cells/2 mL/well and cultured with RPMI1640 medium containing B27 supplement (2%), human activin A (100 ng/mL), CHIR99021 (1 μ M), and sodium butyrate (0.125 mM) for 6 days. For anteriorization, the cells were differentiated using a DMEM/F12 plus Glutamax medium containing B27 supplement (2%), L-ascorbic acid (0.05 mg/mL), monothioglycerol (0.4 mM), human noggin (100 ng/mL), and SB431542 (10 μ M) for 4 days. Then, the cells were treated with DMEM/F12 plus Glutamax medium containing B27 supplement (2%), L-ascorbic acid (0.05 mg/mL), monothioglycerol (0.4 mM), human BMP4 (20 ng/mL), ATRA (0.05 μ M), and CHIR99021 (3 μ M) for additional 4 days to

differentiated into ventralized anterior foregut endoderms (VAFEs). VAFEs were further cultured with human FGF10 (10 ng/mL), human KGF (10 ng/mL), CHIR99021 (3 μ M), and DAPT (20 μ M) for 7 days. On differentiation day 21, the cells were detached with Accutase and seeded onto an ultra-low attachment 96-well U-bottom plate at 2×10^5 cells/250 μ L/well to generate fibroblast-free lung spheroids. After 2 days, spheroids were gently collected and resuspended in 20 μ L of human lung normal organoid medium (hLuN medium; Organoid Sciences) mixed with precooled Matrigel at a ratio of 1:1. The drop was embedded onto a 48-well plate to form a 3D culture environment and cultured with 200 μ L of hLuN medium in the presence of Y27632 (10 μ M). The hLuN medium was changed every 2 days. Embedded spheroids matured into hLOs by passaging every 5 - 7 days.

Passage of hLOs

To passage hLOs, culture medium was aspirated from each well, and the Matrigel domes were mechanically disrupted using a 200 μ L pipette tip. hLOs were collected by adding PBS, followed by centrifugation at 5,000 rpm for 30 s, and the supernatant was discarded. The collected hLOs were incubated with Gentle Cell Dissociation Reagent (STEMCELL technologies, Vancouver, Canada) at 37°C for 1 min, and then washed once with PBS. The hLOs fragments were gently resuspended in 20 μ L of hLuN medium mixed with precooled Matrigel at a 1:1 ratio. The mixture was plated onto a 48-well plate, and 200 μ L of hLuN medium was added to each well. Mature hLOs were passaged every 5~7 days, depending on their growth.

Irradiation Experiment

For mice model of RIPP, the mice were irradiated once with 14 Gy using a Gammacell 40 lead collimator with a ^{137}Cs γ -ray source (Gammacell 40 Exactor, Nordin International Inc. Ottawa, Canada) at a 0.8 Gy/min dose rate. The mice were anesthetized with Ketamine (80mg/kg body weight) just before irradiation and then were confined in specifically designed plastic jigs and placed such that the thoraces were in a 3 cm diameter field

defined by lead collimators. hLOs were embedded within matrigel domes in 48-well plate and irradiated at a dose of 2, 4, or 8 Gy γ -ray using ^{137}Cs gamma irradiator on day 1. A second dose was administered on Day 3 using the same parameters.

Lung histopathology

The lung was fixed with 10% neutral-buffered formalin for histopathological examination. Lung tissues were dehydrated, gradually soaked in alcohol and xylene, and embedded in paraffin, and cut into 5 μm thick sections. Tissue sections were deparaffinized and stained with H&E (Abcam, Cambridge, UK) for inflammation evaluation and stained with Masson's trichrome blue to show the collagen deposition. The stained sections were digitally scanned using the Motic EasyScan slide scanning system.

Measurement of TGF- β in BAL Fluid

Mice were euthanized using CO₂ asphyxiation at 4 and 6 months after thoracic irradiation. The trachea was cannulated and BAL was obtained by flushing two times with 0.5ml of PBS including with 1mM EDTA and 10% FBS through a tracheal cannula. BAL was centrifuged and supernatant was stored at -80°C for determination of cytokine levels. To activate latent TGF- β in BAL fluid, 100 μl of BAL fluid was mixed with 20 μl of 1 N HCl and neutralized by adding 20 μl of 1.2 N NaOH/0.5 M HEPES. The level of TGF- β was measured using a commercial ELISA kit (Thermo Fisher Scientific) according to the manufacturer's instructions.

Quantitative Real-Time PCR (qRT-PCR)

For GDF-15 expression in the mice lung, lung tissue was homogenated in the TRIzol Reagent (Thermo Fisher Scientific) according to the manufacturer's protocol. To test genes expressed in hLOs, total RNA was extracted from irradiated and control hLOs using the TRIzol Reagent. cDNA was synthesized from 3 μg of total RNA using random primers, dNTP mixture, and MMLV reverse transcriptase (Promega, Madison, WI, USA).

qRT-PCR was performed using the StepOne Real-Time PCR system (Applied Biosystems, Waltham, MA, USA). Primer sequences are listed in Supplementary Table 1. The comparative Ct method was used, and relative mRNA expression was calculated based on normalizing the GAPDH. All reactions were run in triplicate.

Western Blot Analysis

Irradiated and control hLOs were lysed with RIPA buffer. Protein concentrations were determined, and samples were subjected to SDS-PAGE followed by PVDF membrane transfer. Membranes were blocked and incubated with primary antibodies overnight at 4°C, then probed with HRP-conjugated secondary antibodies. Signals were detected using a UVP ChemStudio system (Analytik Jena, Jena, Germany).

Immunofluorescence Staining

hLOs were seeded within Matrigel dome in a 48-well culture plate and incubated with hLuN medium. hLOs were irradiated with 4 Gy γ -ray using Gamma cell-40 on Day 1 and Day 3. The hLOs were fixed with 4% paraformaldehyde for 10 min and permeabilized with PBS containing with 0.3% Triton X-100 (PBST) for 5 min. After blocking with PBST containing 5% bovine serum albumin, the fixed hLOs were incubated with primary antibody at 4°C overnight, and then stained with Alexa fluor 488- or Alexa fluor 568-conjugated secondary antibody for 1 h. F-actin was stained with Alexa fluor 488-conjugated phalloidin for 10 min and the nuclei were counterstained with DAPI for 5 min. Stained whole hLOs were mounted on a concave slide with FUnGI mounting medium⁵² and the slides were examined using a Zeiss LSM 700 confocal fluorescence microscope (Carl Zeiss, Oberkochen, Germany).

Single cell RNA sequencing

Harvested hLOs were enzymatically dissociated with Accutase cell detachment solution (ThermoFisher) into a single cell suspension and then single cells were counted using LUNA-FL™ Automated Fluorescence cell

counter. Single cell 3'-RNA-Seq samples were prepared using cDNA synthesis kit and loaded in the 10 μ Genomics Chromium Controller according to manufacturer protocol. Briefly, single cells are encapsulated in nanoliter-scale Gel Beads-in-Emulsion (GEMs) using a microfluidic device. These GEMs are generated combining barcoded single cell 3' V3.1 gel beads, reverse transcription (RT) reagents, the single cells, and partitioning oil onto the Chromium Next GEM Chip (Chromium Next GEM Chip G Single Cell Kit). Incubation of the GEMs produces barcoded, full-length cDNA from poly-A mRNA. After RT, GEMs are broken and cDNAs are purified with silane magnetic beads. Then, barcoded full-length cDNA is amplified by PCR to generate enough material for library construction. Amplified cDNA is purified again, and cDNA quality was determined by capillary electrophoresis (Agilent Bioanalyzer). Finally, libraries were sequenced on a NovaSeq 6000 sequencer (Illumina). Each measurement comes from independent normal and irradiated hLOs.

Statistics

All experiments were independently repeated at least three times. Data are expressed as mean \pm standard deviation (SD). Statistical significance was evaluated using two-tailed unpaired Student's t-tests. A *p*-value < 0.05 was considered statistically significant.

Data availability

The datasets generated during and/or analyzed during the current study are available from the corresponding author on reasonable request. FASTQ was generated using Novaseq6000, and processed data (Matrix, etc.) were produced using CellRanger pipeline Ver. 8.0.1. The original raw data and the processing data utilized in this study have been deposited into the National Library of Medicine. The BioProject accession number is PRJNA1294537 and the BioSample accession number is SAMN50098139 (Normal) and SAMN50098140 (Irradiation).

References

- 1 Arroyo-Hernandez, M. *et al.* Radiation-induced lung injury: current evidence. *BMC Pulm. Med.* **21**, 9, doi:10.1186/s12890-020-01376-4 (2021).
- 2 Wynn, T. A. & Ramalingam, T. R. Mechanisms of fibrosis: therapeutic translation for fibrotic disease. *Nat. Med.* **18**, 1028-1040, doi:doi.org/10.1038/nm.2807 (2012).
- 3 Yan, Y. *et al.* Exploration of radiation-induced lung injury, from mechanism to treatment: a narrative review. *Transl. Lung Cancer Res.* **11**, 307-322, doi:10.21037/tlcr-22-108 (2022).
- 4 Huang, Y., Zhang, W., Yu, F. & Gao, F. The cellular and molecular mechanism of radiation-induced lung injury. *Med. Sci. Monit.* **23**, 3446-3450, doi:10.12659/msm.902353 (2017).
- 5 Jarzebska, N. *et al.* Scarred lung. An update on radiation-induced pulmonary fibrosis. *Front. Med.* **7**, 585756, doi:10.3389/fmed.2020.585756 (2020).
- 6 Mehta, V. Radiation pneumonitis and pulmonary fibrosis in non-small-cell lung cancer: Pulmonary function, prediction, and prevention. *Int. J. Radiat. Oncol. Biol. Phys.* **63**, 5-24, doi:10.1016/j.ijrobp.2005.03.047 (2005).
- 7 Käsmann, L. *et al.* Radiation-induced lung toxicity - cellular and molecular mechanisms of pathogenesis, management, and literature review. *Radiat. Oncol.* **15**, 214, doi:10.1186/s13014-020-01654-9 (2020).
- 8 Liu, G. Y., Budinger, G. S. & Dematte, J. E. Advances in the management of idiopathic pulmonary fibrosis and progressive pulmonary fibrosis. *BMJ* **377**, e066354, doi:10.1136/bmj-2021-066354 (2022).
- 9 Bonella, F., Spagnolo, P. & Ryerson, C. Current and future treatment landscape for idiopathic pulmonary fibrosis. *Drugs* **83**, 1581-1593, doi:10.1007/s40265-023-01950-0 (2023).
- 10 Cogno, N., Bauer, R. & Durante, M. An agent-based model of

- radiation-induced lung fibrosis. *Int. J. Mol. Sci.* **23**, 13920, doi:10.3390/ijms232213920 (2022).
- 11 11 Fatehullah, A., Tan, S. H. & Barker, N. Organoids as an in vitro model of human development and disease. *Nat. Cell Biol.* **18**, 246-254, doi:10.1038/ncb3312 (2016).
- 12 12 Kumar, D. *et al.* Development and characterization of an in vitro model for radiation-induced fibrosis. *Radiat. Res.* **189**, 326-336, doi:10.1667/RR14926.1 (2018).
- 13 13 Corona, C., Man, K., Newton, C. A., Nguyen, K. T. & Yang, Y. In vitro modeling of idiopathic pulmonary fibrosis: Lung-on-a-chip systems and other 3D cultures. *Int. J. Mol. Sci.* **25**, 11751, doi:10.3390/ijms252111751 (2024).
- 14 14 Cooper, J. R. *et al.* Long term culture of the A549 cancer cell line promotes multilamellar body formation and differentiation towards an alveolar type II pneumocyte phenotype. *PLoS One* **11**, e0164438, doi:10.1371/journal.pone.0164438 (2016).
- 15 15 Korrodi-Gregorio, L., Soto-Cerrato, V., Vitorino, R., Fardilha, M. & Perez-Tomas, R. From proteomic analysis to potential therapeutic targets: Functional profile of two lung cancer cell lines, A549 and SW900, widely studied in pre-clinical research. *PLoS One* **11**, e0165973, doi:10.1371/journal.pone.0165973 (2016).
- 16 16 Gul, A. *et al.* Pulmonary fibrosis model of mice induced by different administration methods of bleomycin. *BMC Pulm. Med.* **23**, 91, doi:10.1186/s12890-023-02349-z (2023).
- 17 17 Tabata, C. *et al.* All-trans-retinoic acid prevents radiation- or bleomycin-induced pulmonary fibrosis. *Am. J. Respir. Crit. Care Med.* **174**, 1352-1360, doi:10.1164/rccm.200606-862OC (2006).
- 18 18 Jin, H. *et al.* Radiation-induced lung fibrosis: preclinical animal models and therapeutic strategies. *Cancers* **12**, 1561, doi:10.3390/cancers12061561 (2020).
- 19 19 McIlrath, D. R., Roach, E., Porro, G. & Perez-Torres, C. J. Feasibility of quantification of murine radiation-induced pulmonary fibrosis

- with microCT imaging. *J. Radiat. Res.* **62**, 976-981, doi:10.1093/jrr/rrab096 (2021).
- 20 Kumar, V. P. *et al.* Development of a radiation-induce pulmonary fibrosis partial body irradiation model in C57BL/6 mice. *Radiat. Res.* **201**, 460-470, doi:10.1667/RADE-23-00143.1 (2024).
- 21 Dasgupta, Q. *et al.* A human lung alveolus-on-a-chip model of acute radiation-induced lung injury. *Nat. Commun.* **14**, 6506, doi:10.1038/s41467-023-42171-z (2023).
- 22 Cussac, L. A. *et al.* TRPV4 channel mediates adventitial fibroblast activation and adventitial remodeling in pulmonary hypertension. *Am. J. Physiol. Lung Cell. Mol. Physiol.* **318**, L135-L146, doi:10.1152/ajplung.00084.2019 (2020).
- 23 Koziol-White, C., Gebski, E., Cao, G. & Panettieri, R. A., Jr. Precision cut lung slices: an integrated ex vivo model for studying lung physiology, pharmacology, disease pathogenesis and drug discovery. *Radiat. Res.* **25**, 231, doi:10.1186/s12931-024-02855-6 (2024).
- 24 Vazquez-Armendariz, A. I., Barroso, M. M., El Agha, E. & Herold, S. 3D In Vitro Models: Novel Insights into Idiopathic Pulmonary Fibrosis Pathophysiology and Drug Screening. *Cells* **11**, 1526, doi:10.3390/cells11091526 (2022).
- 25 Vazquez-Armendariz, A. I. & Tata, P. R. Recent advances in lung organoid development and applications in disease modeling. *J. Clin. Invest.* **133**, e170500, doi:10.1172/JCI170500 (2023).
- 26 Leko, I. M. *et al.* A distal lung organoid model to study interstitial lung disease, viral infection and human lung development. *Nat. Protoc.* **18**, 2283-2312, doi:10.1038/s41596-023-00827-6 (2023).
- 27 Oglesby, I. K. *et al.* Lung organoids and other preclinical models of pulmonary fibrosis. *QJM* **114**, 167-173, doi:10.1093/qjmed/hcaa281 (2021).
- 28 Quan, Y. *et al.* Organ-on-a-chip: the next generation platform for risk assessment of radiobiology. *RSC Adv.* **10**, 39521-39530, doi:10.1039/d0ra05173j (2020).

- 29 Yamamoto, Y., Korogi, Y., Hirai, T. & Gotoh, S. in *Methods in cell biology* Vol. 159 (ed Jason R. Spence) 115-141 (Elsevier, 2020).
- 30 Xie, T. *et al.* Abnormal respiratory progenitors in fibrotic lung injury. *Stem Cell Res. Ther.* **13**, 64, doi:10.1186/s13287-022-02737-y (2022).
- 31 N. Lekkerkerker, A., Aarbiou, J., van Es, T. & A.J. Janssen, R. Cellular players in lung fibrosis. *Curr. Pharm. Des.* **18**, 4093-4102, doi:10.2174/138161212802430396 (2012).
- 32 Henderson, N. C., Rieder, F. & Wynn, T. A. Fibrosis: from mechanisms to medicines. *Nature* **587**, 555-566, doi:10.1038/s41586-020-2938-9 (2020).
- 33 Munger, J. S. *et al.* The Integrin $\alpha v\beta 6$ Binds and Activates Latent TGF $\beta 1$: A Mechanism for Regulating Pulmonary Inflammation and Fibrosis. *Cell* **96**, 319-328, doi:10.1016/S0092-8674(00)80545-0 (1999).
- 34 Radwanska, A. *et al.* Increased expression and accumulation of GDF15 in IPF extracellular matrix contribute to fibrosis. *JCI Insight* **7**, e153058, doi:10.1172/jci.insight.153058 (2022).
- 35 Zhang, Y. *et al.* GDF15 is an epithelial-derived biomarker of idiopathic pulmonary fibrosis. *Am. J. Physiol. Lung Cell. Mol. Physiol.* **317**, L510-L521, doi:10.1152/ajplung.00062.2019 (2019).
- 36 Boström, H. *et al.* PDGF-A signaling is a critical event in lung alveolar myofibroblast development and alveogenesis. *Cell* **85**, 863-873, doi:10.1016/S0092-8674(00)81270-2 (1996).
- 37 Li, J. & Hoyle, G. W. Overexpression of PDGF-A in the lung epithelium of transgenic mice produces a lethal phenotype associated with hyperplasia of mesenchymal cells. *Dev. Biol.* **239**, 338-349, doi:10.1006/dbio.2001.0441 (2001).
- 38 Shah, P. V. *et al.* A Review of Pirfenidone as an Anti-Fibrotic in Idiopathic Pulmonary Fibrosis and Its Probable Role in Other Diseases. *Cureus* **13**, e12482, doi:10.7759/cureus.12482 (2021).
- 39 Komiya, C. *et al.* Antifibrotic effect of pirfenidone in a mouse model of human nonalcoholic steatohepatitis. *Sci. Rep.* **7**, 44754,

- doi:10.1038/srep44754 (2017).
- 40 Zhou, S., Zhu, J., Zhou, P.-K. & Gu, Y. Alveolar type 2 epithelial cell senescence and radiation-induced pulmonary fibrosis. *Front. Cell Dev. Biol.* **10**, 999600, doi:10.3389/fcell.2022.999600 (2022).
- 41 Luo, L. *et al.* The role of epithelial cells in fibrosis: Mechanisms and treatment. *Pharmacol. Res.* **202**, 107144, doi:10.1016/j.phrs.2024.107144 (2024).
- 42 Huang, R. X. & Zhou, P. K. DNA damage response signaling pathways and targets for radiotherapy sensitization in cancer. *Signal Transduct. Target. Ther.* **5**, 60, doi:10.1038/s41392-020-0150-x (2020).
- 43 Ohta, H., Chiba, S., Ebina, M., Furuse, M. & Nukiwa, T. Altered expression of tight junction molecules in alveolar septa in lung injury and fibrosis. *Am. J. Physiol. Lung Cell. Mol. Physiol.* **302**, L193-L205, doi:10.1152/ajplung.00349.2010 (2012).
- 44 Nagarajan, D., Melo, T., Deng, Z., Almeida, C. & Zhao, W. ERK/GSK3beta/Snail signaling mediates radiation-induced alveolar epithelial-to-mesenchymal transition. *Free Radic. Biol. Med.* **52**, 983-992, doi:10.1016/j.freeradbiomed.2011.11.024 (2012).
- 45 Citrin, D. E. *et al.* Role of type II pneumocyte senescence in radiation-induced lung fibrosis. *J. Natl. Cancer Inst.* **105**, 1474-1484, doi:10.1093/jnci/djt212 (2013).
- 46 Wang, L. K. *et al.* Radiation induces pulmonary fibrosis by promoting the fibrogenic differentiation of alveolar stem cells. *Stem Cells Int.* **2020**, 6312053, doi:10.1155/2020/6312053 (2020).
- 47 Diebold, L. P. & Jain, M. Pulmonary fibrosis and antioxidants: Finding the right target. *Am. J. Respir. Cell Mol. Biol.* **69**, 3-5, doi:10.1165/rcmb.2023-0110ED (2023).
- 48 Wynn, T. A. Cellular and molecular mechanisms of fibrosis. *J. Pathol.* **214**, 199-210, doi:10.1002/path.2277 (2008).
- 49 Park, H.-R., Jo, S.-K. & Jung, U. Thoracic irradiation recruit M2 macrophage into the lung, leading to pneumonitis and pulmonary

- fibrosis. *J. Radiat. Prot. Res.* **42**, 177-188, doi:10.14407/jrpr.2017.42.4.177 (2017).
- 50 Joo, H., Min, S. & Cho, S.-W. Advanced lung organoids for respiratory system and pulmonary disease modeling. *J. Tissue Eng.* **15**, 1-24, doi:10.1177/20417314241232502 (2024).
- 51 Heo, H. R. & Hong, S. H. Generation of macrophage containing alveolar organoids derived from human pluripotent stem cells for pulmonary fibrosis modeling and drug efficacy testing. *Cell Biosci.* **11**, 216, doi:10.1186/s13578-021-00721-2 (2021).
- 52 Rios, A. C. *et al.* Intraclonal plasticity in mammary tumors revealed through large-scale single-cell resolution 3D imaging. *Can. Cell* **15**, 618-632.e6, doi: 10.1016/j.ccell.2019.02.010 (2019).

Acknowledgments

We acknowledge the OrgaonidSciences Inc. for their support in making the lung organoid from human embryonic stem cells for this study. This work was supported by the Korea Research Institute for Defense Technology Planning and Advancement (KRIT) and funded by Defense Acquisition Program Administration (DAPA, KRIT-CT-23-043).

Author Information

Hae-Ran Park and Yeongkag Kwon contributed equally to this work; author order was determined in order of increasing seniority.

Authors and Affiliations

Cyclotron Applied Research Section, Advanced Radiation Technology Institute, Korea Atomic Energy Research Institute (KAERI), Jeongeup 56212, Republic of Korea

Hae-Ran Park, Yeongkag Kwon, Hyun Jung Ji, Minkyu Kim & Kibum Ahn

Cyclotron Applied Research Section, Advanced Radiation Technology Institute, Korea Atomic Energy Research Institute (KAERI), Jeongeup 56212, Republic of Korea

School of Biological Sciences and Institute of Microbiology, Seoul National University, Seoul, 08826, Republic of Korea

Sung Young Kim

Cyclotron Applied Research Section, Advanced Radiation Technology Institute, Korea Atomic Energy Research Institute (KAERI), Jeongeup 56212, Republic of Korea

Department of Radiation Science, University of Science and Technology, Daejeon, Republic of Korea

Ho Seong Seo

Contributions

The authors confirm contribution to the paper as follows: YK and HRP carried out all *in vitro* and *in vivo* experiments and wrote the manuscript. HHJ and SYK helped to perform immunofluorescence staining. MK and KA assisted in interpreting the scRNAseq results. HRP and HSS participated in the design of study. All authors reviewed the results and approved the final version of the manuscript.

Corresponding Authors

Correspondence to Ho Seong Seo & Hae-Ran Park

Ethics declarations

Competing Interests

The authors declare that they have no competing interests.

Ethical approval

This study was performed in accordance with the ARRIVE guidelines and was conducted in accordance with the guidelines of the National Institutes of Health Guide for the Care and Use of Laboratory Animals. Experimental protocols were approved by the Institutional Animal Care and Use Committee of the Korea Atomic Energy Research Institute (KAERI; approval no. KAERI-IACUC-2024-008). All experiments were performed at the RI-BIOMICS facility (Jeongeup, Republic of Korea) under standard veterinary care practices.

Clinical trial number

Not applicable.

Consent for publication

Informed consent was obtained from all individual participants included in the study.

ARTICLE IN PRESS

Figure Legends

Figure 1. Generation and characterization of human lung organoids derived from hESCs. (A) Representative phase-contrast images showing human embryonic stem cells (hESCs) on day 1 of culture and mature lung organoids (hLOs) after differentiation. (B) Relative mRNA expression levels of lung epithelial cell markers, including podoplanin (PDPN, AT1 cell marker), surfactant protein A1 (SFTPA1, AT2 cell marker), secretoglobin family 1A member 1 (SCGB1A1/CC10, club cell marker), mucin 5AC (Muc5AC, goblet cell marker), and tumor protein p63 (TP63, basal cell marker), as determined by quantitative real-time RT-PCR. Values were normalized to GAPDH expression. (C) Immunofluorescence staining of mature hLOs showing cell-type-specific markers. Organoids were stained with antibodies against CC10 (green, club cells), PDPN (red, AT1 cells), SFTPA1 (green, AT2 cells), and Muc5AC (red, goblet cells). Nuclei were counterstained with DAPI (blue). Merged images confirm the presence of multiple lung epithelial lineages within the organoids. Images were captured using confocal laser scanning microscopy. Scale bar = 25 μ m.

Figure 2. Ionizing radiation inhibits growth and proliferation of human lung organoids (hLOs). (A) Schematic overview of the irradiation protocol. hLOs embedded in Matrigel were irradiated with 2, 4, or 8 Gy γ -rays using a ^{137}Cs source on Day 1, followed by a second identical dose on Day 4. Organoid size and proliferative activity were assessed on Day 5. (B) Representative phase-contrast images showing control (left) and irradiated (right) hLOs. (C) Quantification of organoid size. Diameter measurements were obtained from multiple hLOs under each condition using inverted microscopy. Error bars indicate standard deviation ($n=60$). (D) Immunofluorescence images of hLOs stained for Ki-67 (red), F-actin (phalloidin; white), and nuclei (DAPI; blue) to assess proliferative activity. All images were captured using confocal laser scanning microscopy. Scale bar = 50 μ m. (E) Quantification of Ki-67 $^+$ cells per organoid in control versus irradiated groups. Each dot represents one organoid. Statistical analysis was performed using an unpaired two-tailed

t-test. * $p < 0.005$, ** $p < 0.001$ compared with non-irradiated control.

Figure 3. Single-cell RNA sequencing reveals radiation-induced alterations in epithelial subpopulations within hLOs. (A) Uniform Manifold Approximation and Projection (UMAP) plots visualizing cell clusters derived from control (left) and irradiated (4 Gy \times 2) hLOs (right), based on 10 \times Genomics single-cell RNA sequencing. Distinct epithelial subtypes were identified and annotated: proliferating AT2 cells, AT2 cells, AT1 cells, ciliated cells, club cells, goblet cells, basal cells, and rare cells. Cluster identities were determined by expression of canonical marker genes shown in the accompanying dot plot (right), where dot size indicates the percentage of cells expressing each gene and color intensity represents average expression level. (B) Donut plots showing proportional changes in epithelial subtypes between control and irradiated hLOs. Notably, proliferating AT2 cells decreased, while basal and ciliated cell populations increased following radiation. (C) Quantification of total and relative cell counts for each epithelial subtype in control and irradiated conditions, highlighting shifts in cellular composition following γ -ray exposure.

Figure 4. Ionizing radiation induces EMT-like changes and upregulation of α -SMA in hLOs. (A) Western blot analysis showing changes in epithelial and mesenchymal marker expression following a single or repeated γ -ray irradiation (2, 4, or 8 Gy) of hLOs. Irradiated hLOs exhibited decreased expression of epithelial markers (E-cadherin, occludin) and increased expression of mesenchymal proteins (N-cadherin, vimentin, α -SMA, collagen III). β -actin was used as a loading control. (B) Representative immunofluorescence images of hLOs stained for E-cadherin (red), N-cadherin (green), and DAPI (blue) to visualize EMT-associated structural changes. Scale bar = 50 μ m. (C) Quantitative RT-PCR analysis of α -smooth muscle actin (α -SMA) mRNA levels in hLOs exposed to increasing doses of γ -irradiation, either once or twice. Bars represent mean \pm SD ($n = 3$). * $p < 0.05$, ** $p < 0.001$ compared with non-irradiated control. (D) Immunofluorescence staining of α -SMA protein (red)

in hLOs confirms radiation-induced myofibroblastic differentiation. Nuclei were counterstained with DAPI (blue). All images were captured using confocal laser scanning microscopy. Scale bar = 50 μ m.

Figure 5. Ionizing radiation induces extracellular matrix (ECM) accumulation in the lung of mice and in hLOs. (A) Schematic overview of the thoracic irradiation protocol in mice. C57BL/6 female mice were irradiated on the thorax at the dose of 14 Gy. The lung was harvested 4- and 6-months post-irradiation. (B) Representative H&E staining and Masson's trichrome staining of lung tissue. Scale bars is 100 μ m. (C-E) The lung sections stained with H&E were scored for airway, vascular, and parenchymal inflammatory features from to 5 by a broad-certified, blinded pathologist. Bars represent mean \pm SD (n = 5). (F) Ashcroft scores were measured to quantify collagen contents. Bars represent mean \pm SD (n = 5). (G-I) Quantitative RT-PCR analysis of collagen isoforms in hLOs following single or repeated γ -ray irradiation (2, 4, or 8 Gy). mRNA expression levels of (G) COL1A1, (H) COL1A2, and (I) COL3A1 were measured and normalized to GAPDH. Bars represent mean \pm SD (n = 3). (J, K) Representative immunofluorescence images of irradiated hLOs stained for (J) collagen I and (K) collagen III (green), with nuclei counterstained using DAPI (blue). Confocal microscopy revealed enhanced ECM deposition, particularly in intercellular and peripheral regions of hLOs. Scale bar = 50 μ m. Statistical significance was determined using an unpaired two-tailed Student's t-test. *p < 0.05, **p<0.001 compared with non-irradiated control.

Figure 6. Ionizing radiation induces profibrotic cytokine expression in the lung of mice and in hLOs. (A, B) C57BL/6 female mice were irradiated on the thorax at the dose of 14 Gy. At 4- and 6-months post-irradiation, the BAL fluid and the lung homogenates were obtained. The levels of TGF- β (A) in BAL fluid were measured by ELISA and the expression levels of GDF15 (B) were measured by quantitative RT-PCR. (C-E) Quantitative RT-PCR analysis of fibrogenic cytokines in hLOs following single or repeated γ -ray irradiation (2, 4, or 8 Gy). mRNA expression levels

of (C) TGF- β , (D) GDF-15, and (E) PDGF-A were measured and normalized to GAPDH. Bars represent mean \pm SD ($n = 3$). Statistical significance was determined using an unpaired two-tailed Student's t-test. * $p < 0.05$, ** $p < 0.005$, *** $p < 0.001$ compared with non-irradiated control.

Figure 7. Pirfenidone suppresses radiation-induced expression of fibrosis-associated genes in hLOs. (A) Schematic illustration of the anti-fibrosis drug screening experiment. hLOs were irradiated with 4 Gy γ -rays on Day 1 and Day 4. Pirfenidone (PFD, 0.5 mg/mL) was administered immediately after each irradiation. Total RNA was extracted on Day 5 for transcript analysis. (B-D) Quantitative RT-PCR analysis showing relative mRNA expression levels of profibrotic markers, (B) TGF- β , (C) α -SMA, and (D) COL1A2. Expression values were normalized to GAPDH and expressed as fold change relative to non-irradiated controls. Bars represent mean \pm SD ($n = 3$). * $p < 0.05$ compared to PBS-treated irradiated group, assessed by unpaired two-tailed Student's t-test.

Figure 8. Schematic summary of radiation-induced pulmonary fibrosis mechanisms modeled in hLOs. (A) Ionizing radiation induces epithelial damage in human lung organoids (hLO), resulting in impaired proliferation and loss of epithelial integrity, and secretion of profibrotic cytokines such as TGF- β , GDF-15, and PDGF-A from damaged specific epithelial cells. (B) In summary, ionizing radiation caused damage to epithelial cells composing the bronchi and alveoli in hLO, abnormal differentiation through the EMT process, and deposition of excessive ECM, all of which contribute to the pathological cascade of pulmonary fibrosis.

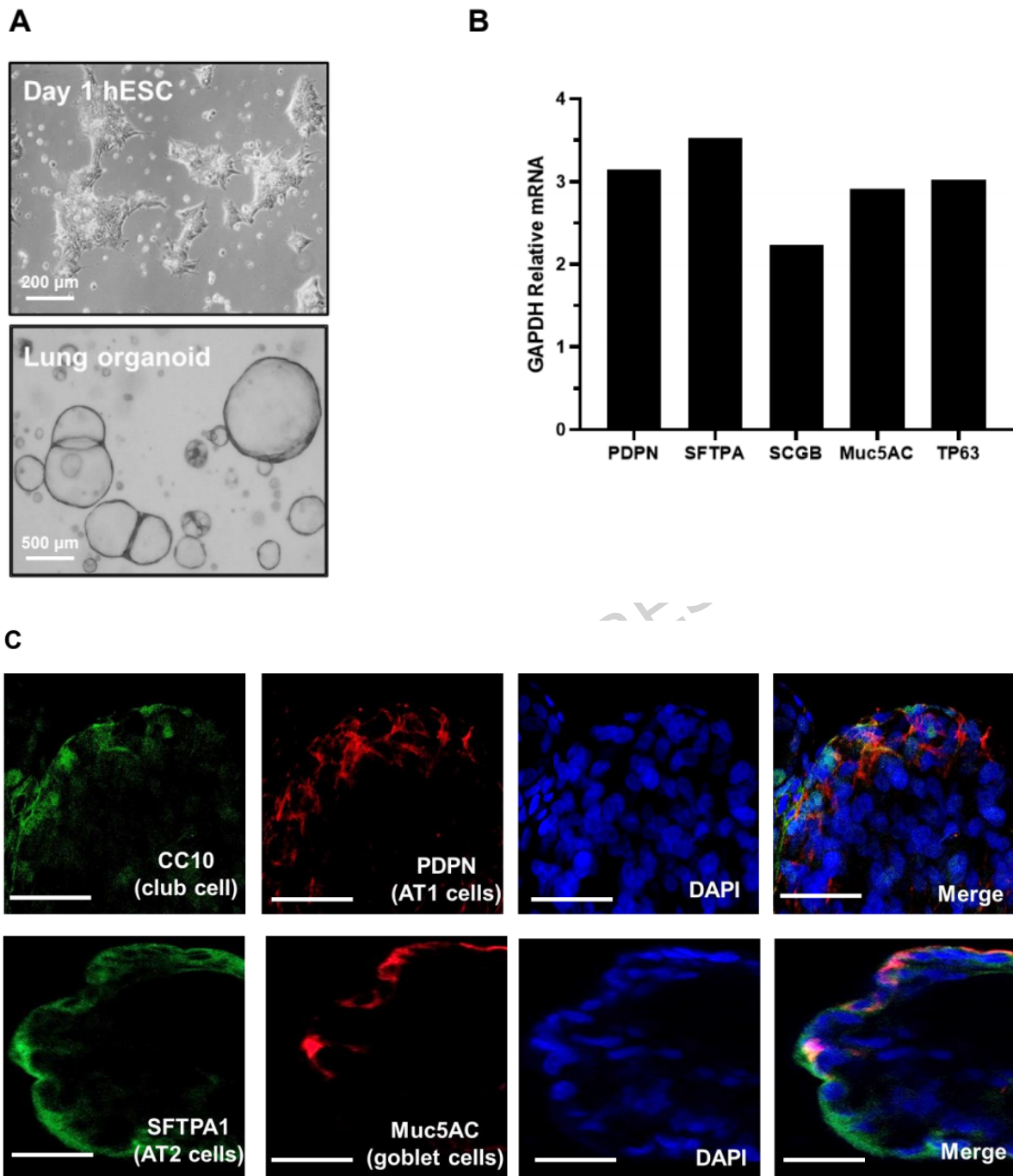
Figure 1.

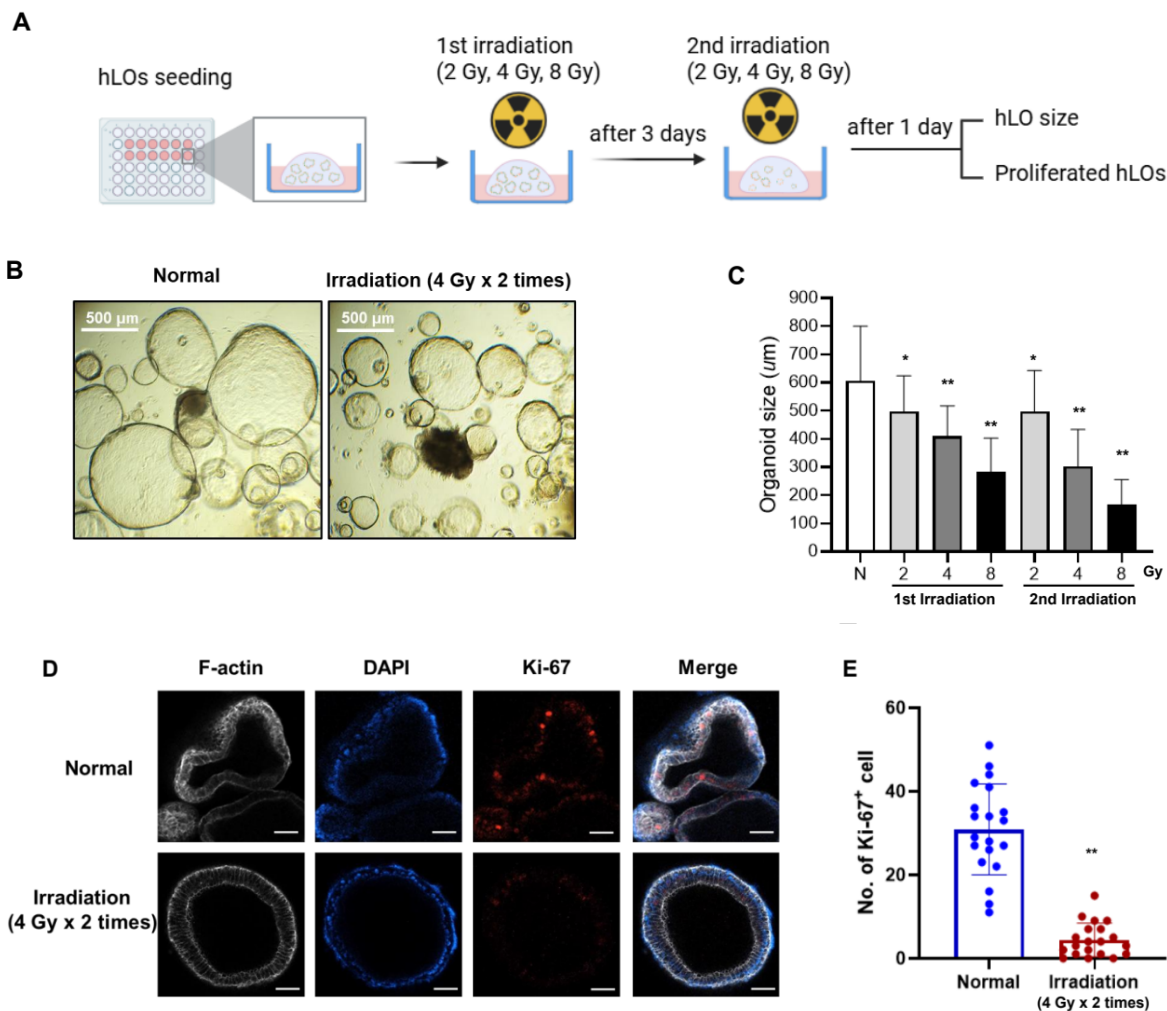
Figure 2.

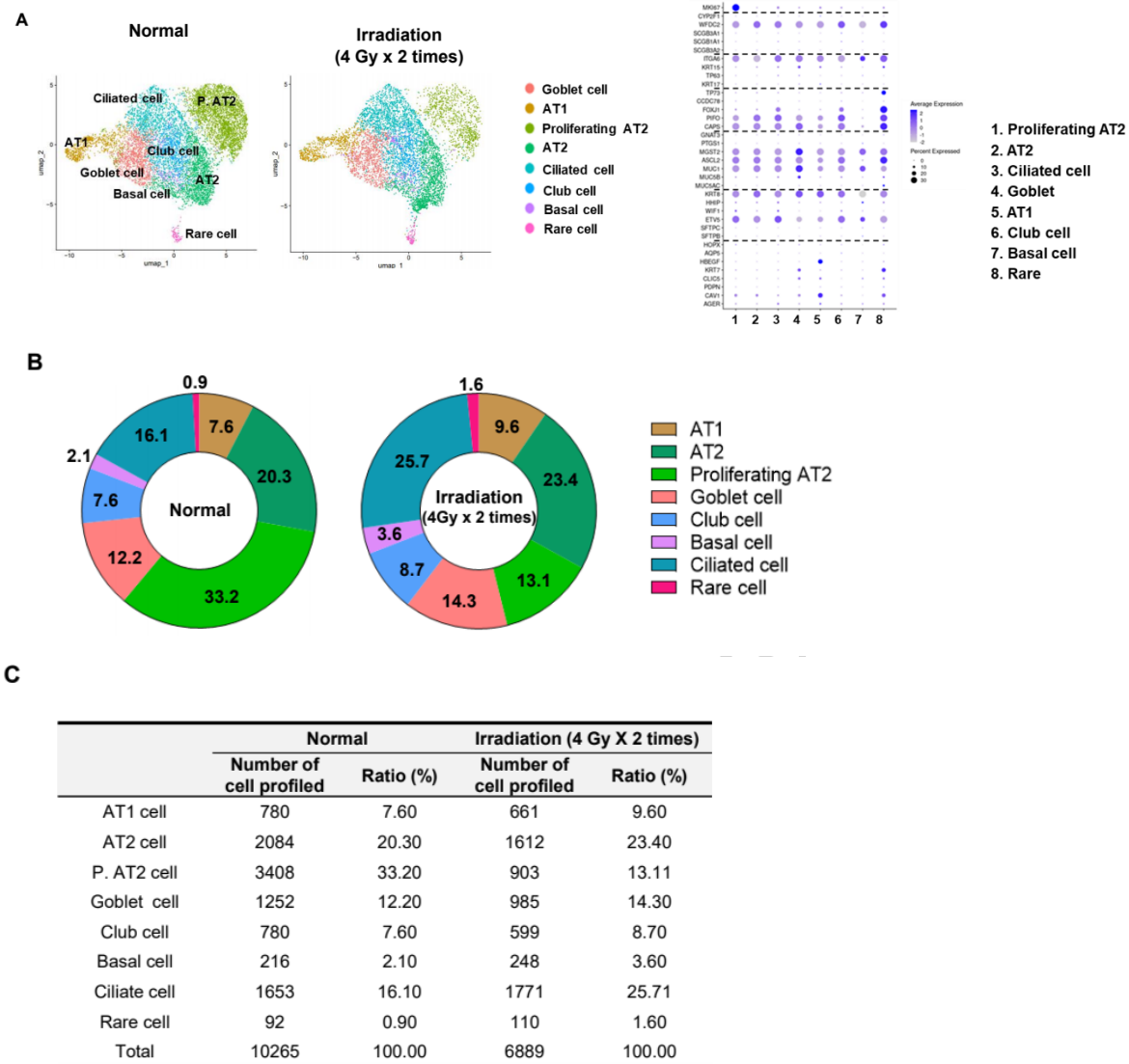
Figure 3.

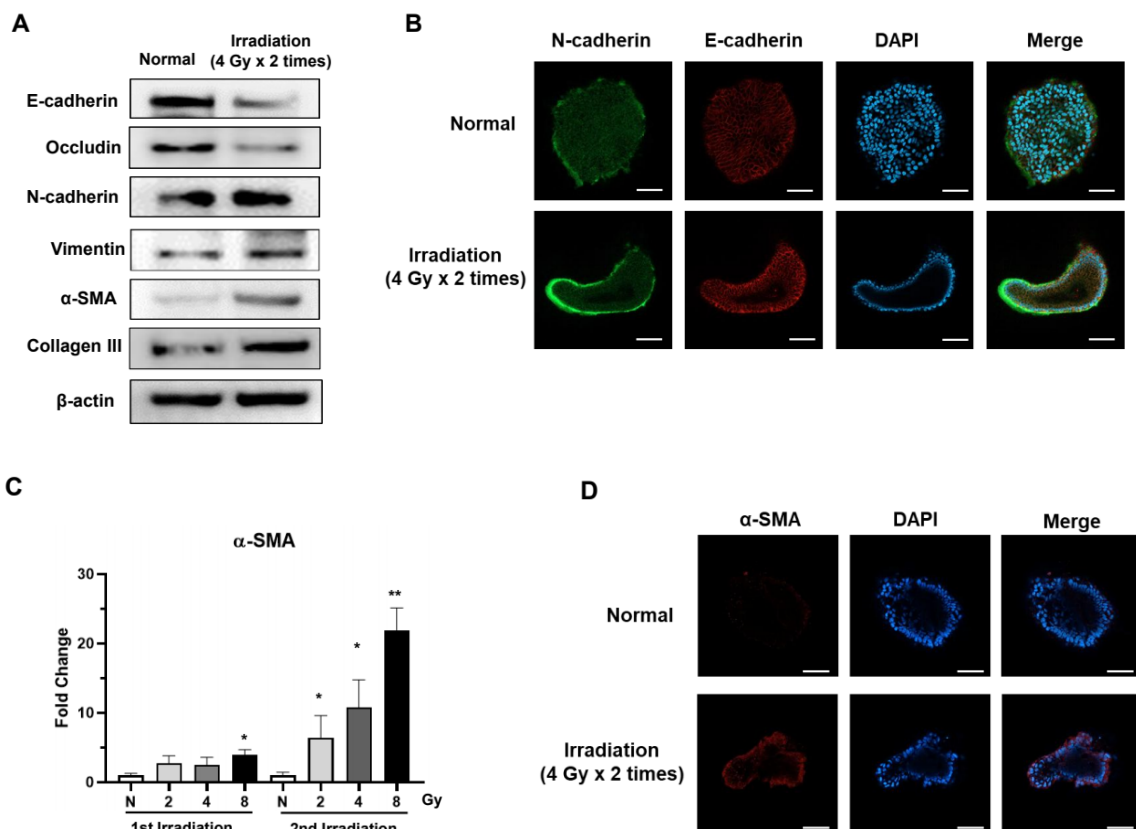
Figure 4.

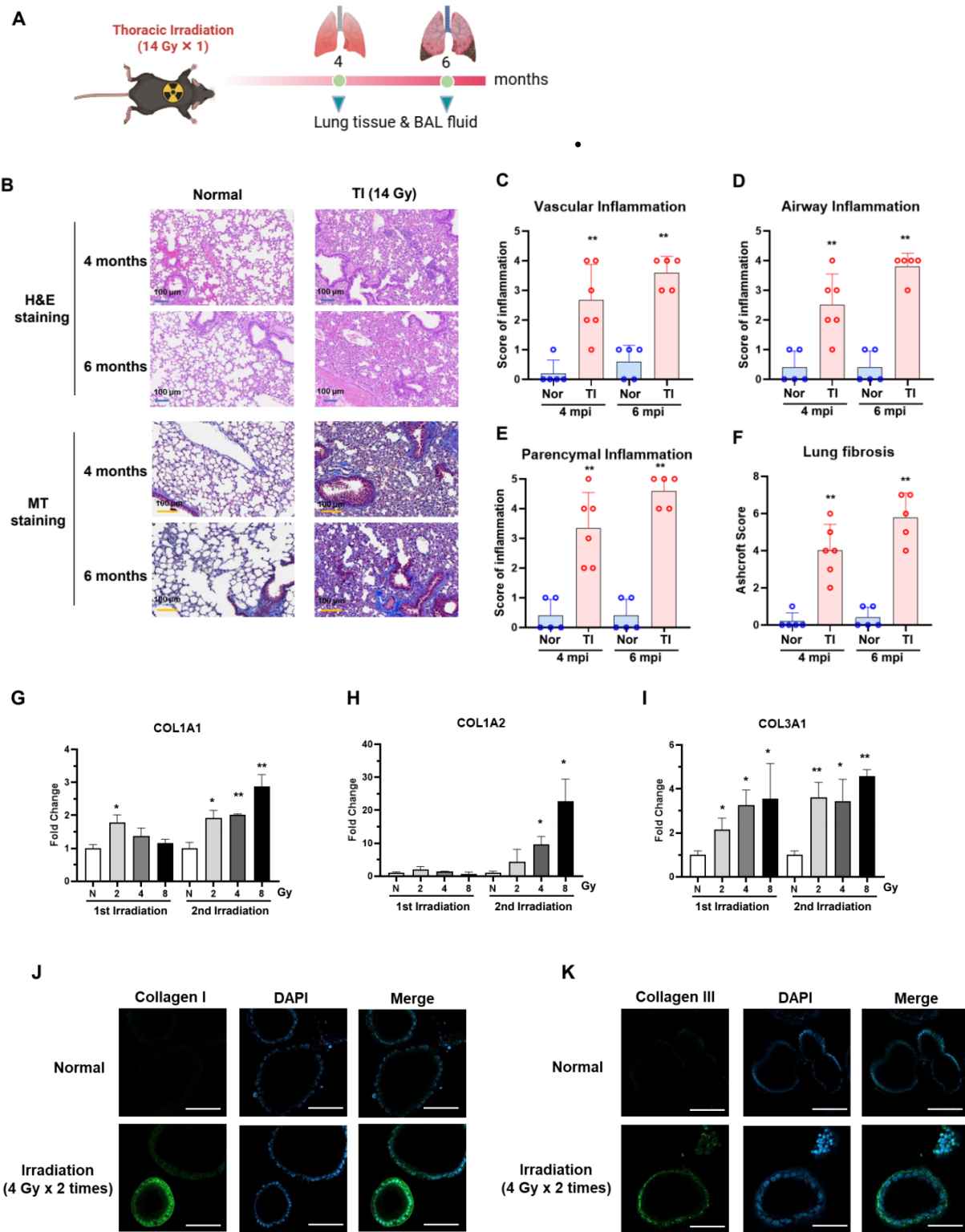
Figure 5.

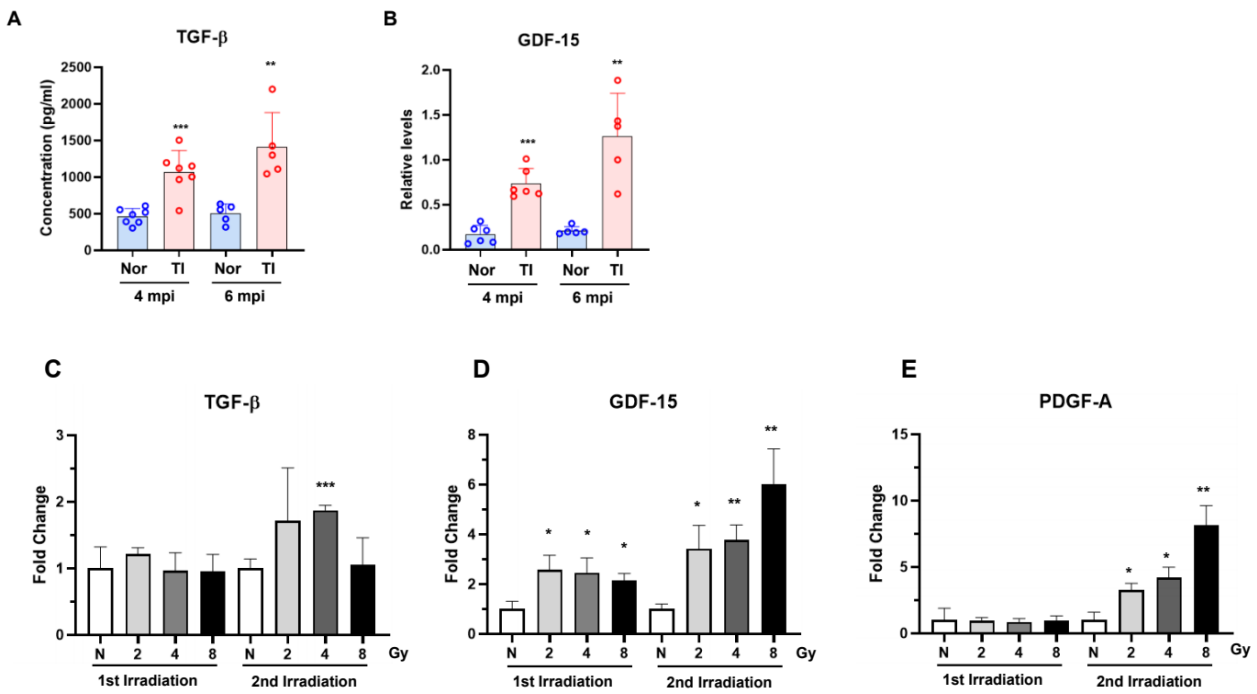
Figure 6.

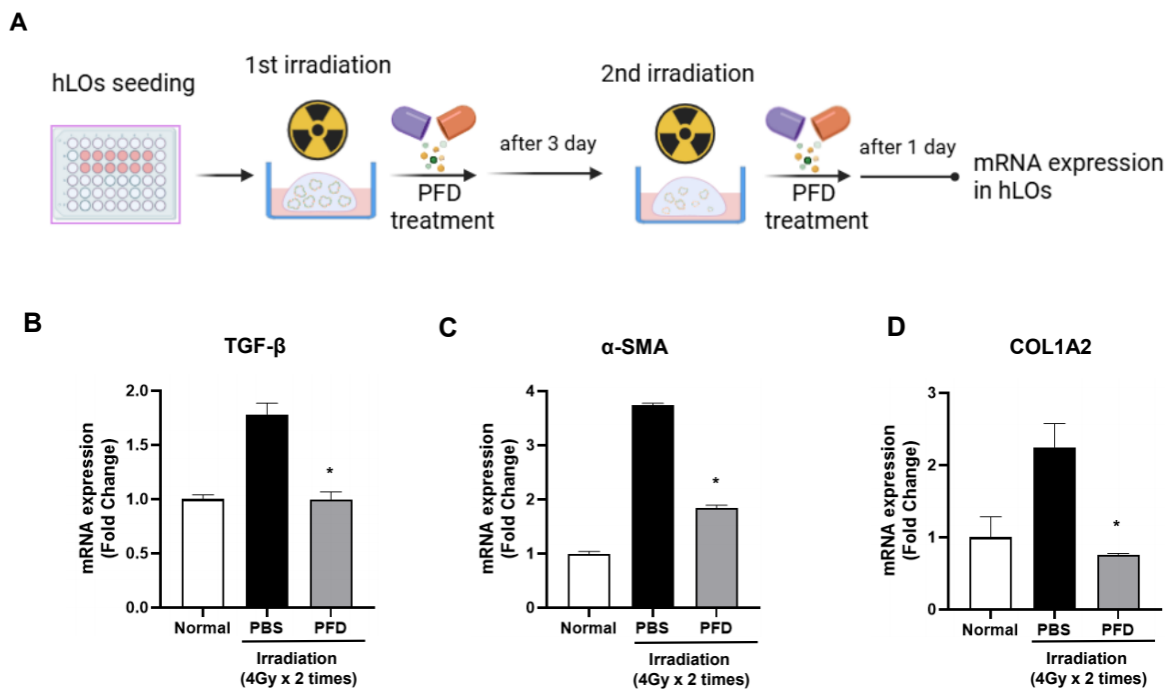
Figure 7.

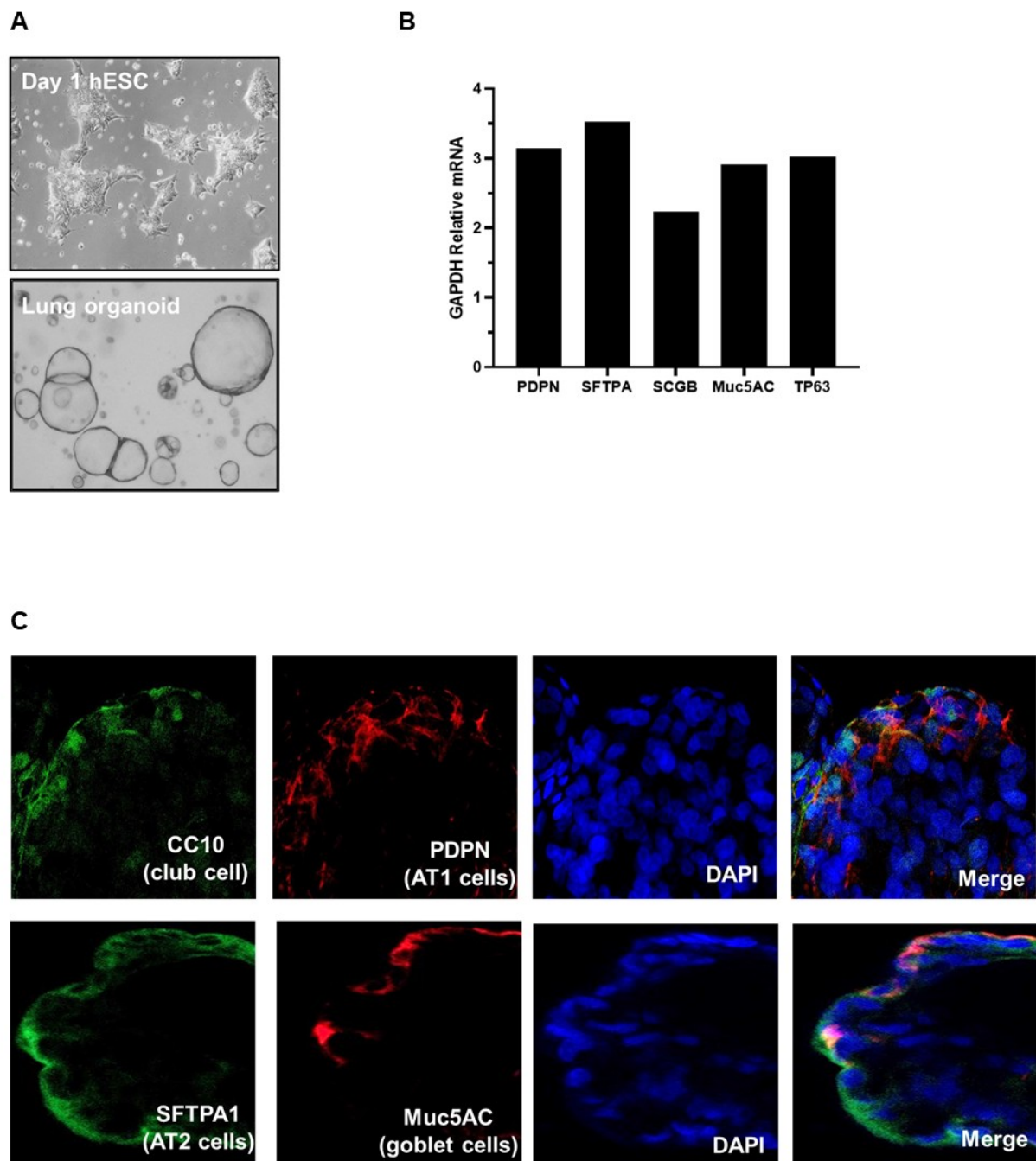
Figure 01

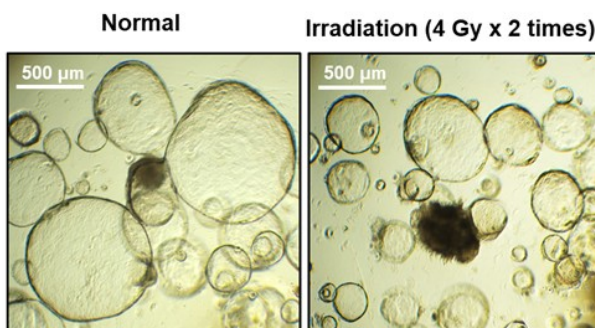
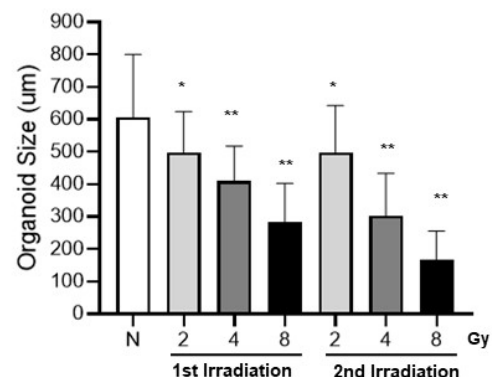
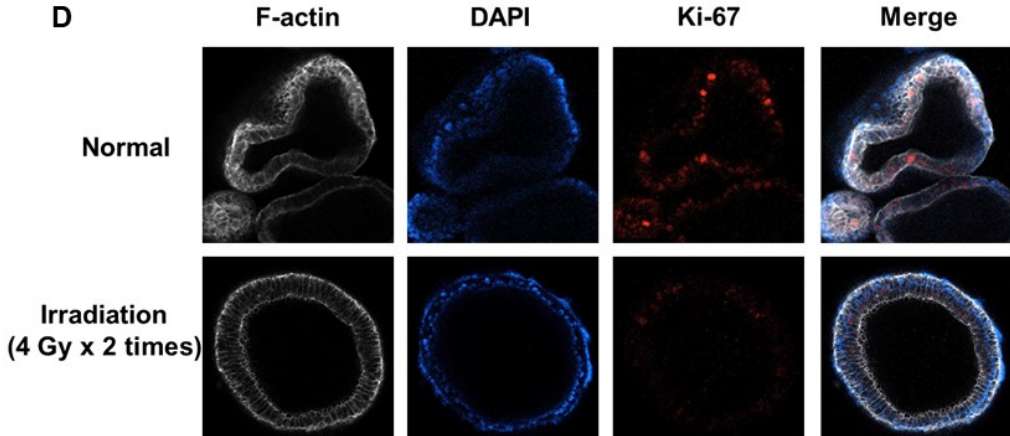
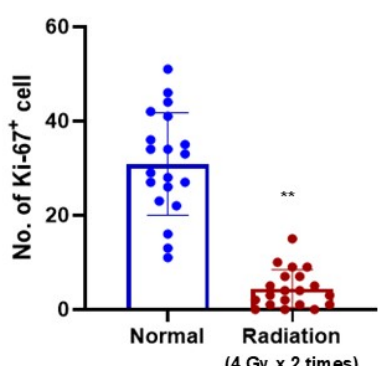
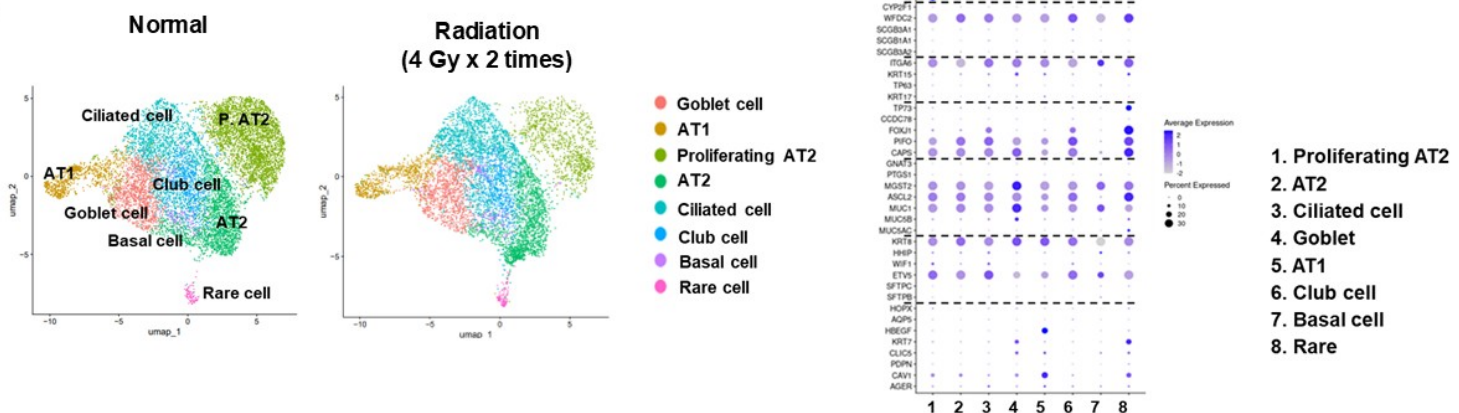
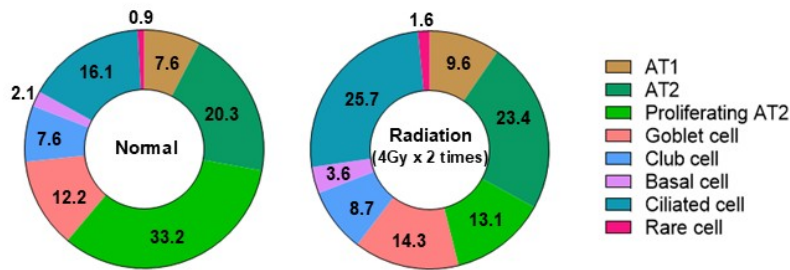
Figure 02**A****B****C****D****E**

Figure 03**A****B****C**

	0 Gy		4 Gy X 2	
	cell number	ratio (%)	cell number	ratio (%)
AT1 cell	780	7.60	661	9.60
AT2 cell	2084	20.30	1612	23.40
P. AT2 cell	3408	33.20	903	13.11
Goblet cell	1252	12.20	985	14.30
Club cell	780	7.60	599	8.70
Basal cell	216	2.10	248	3.60
Ciliate cell	1653	16.10	1771	25.71
Rare cell	92	0.90	110	1.60
Total	10265	100.00	6889	100.00

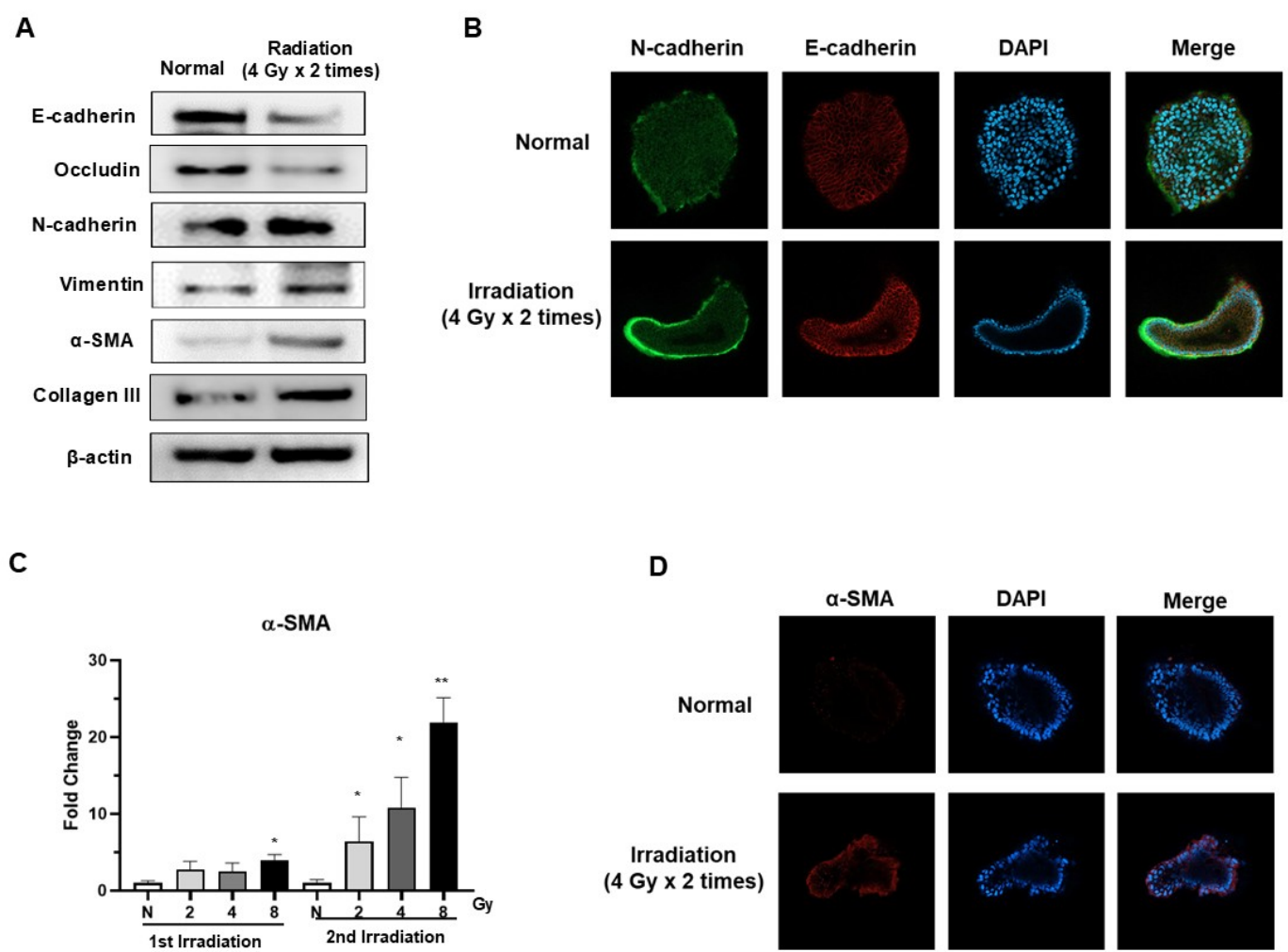
Figure 04

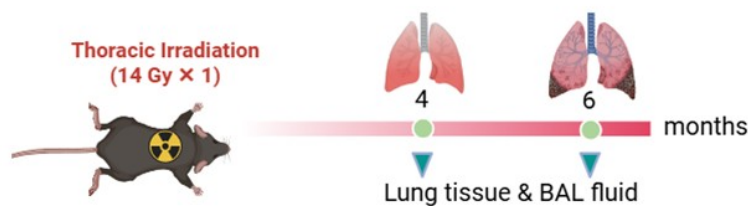
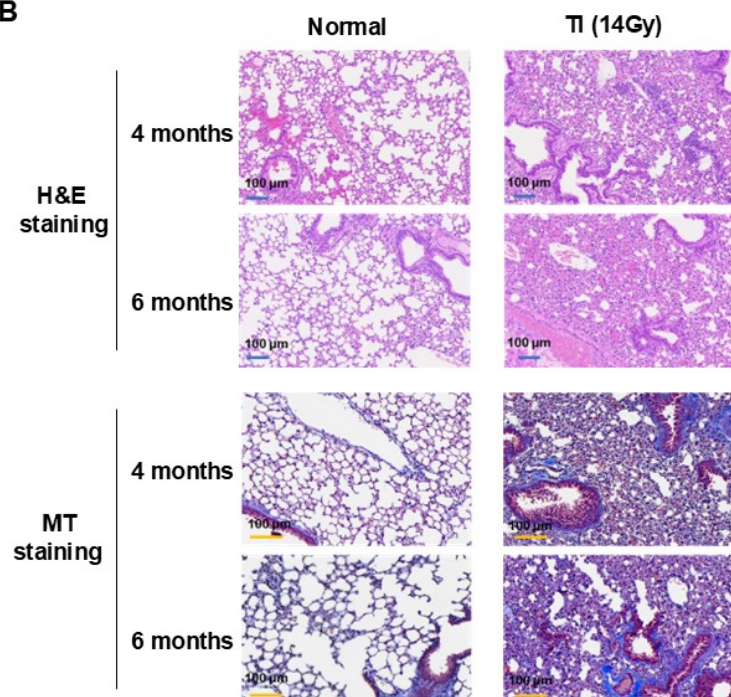
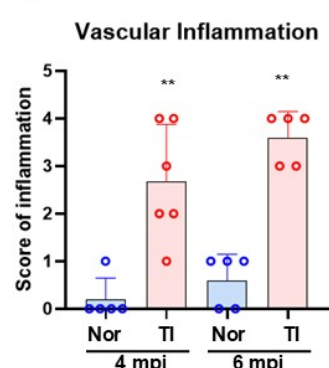
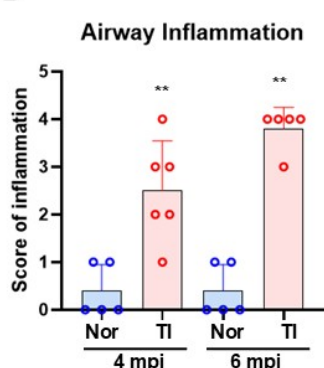
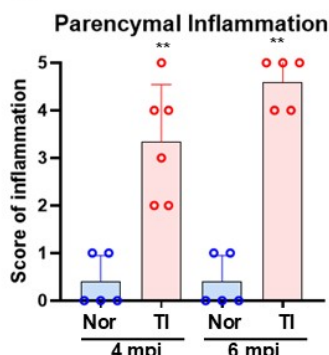
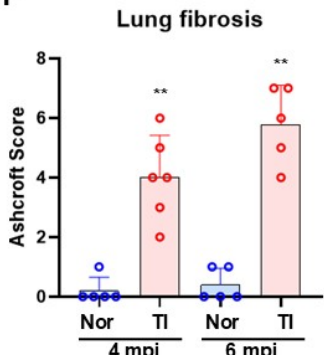
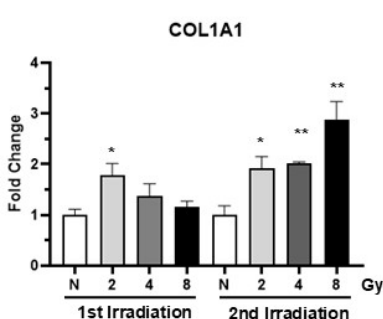
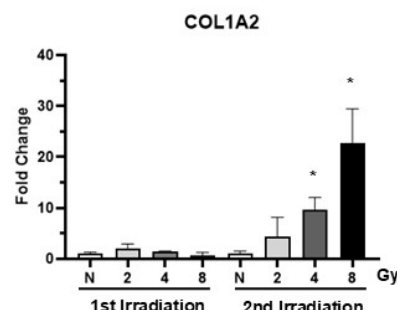
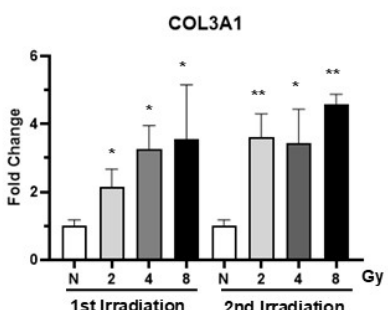
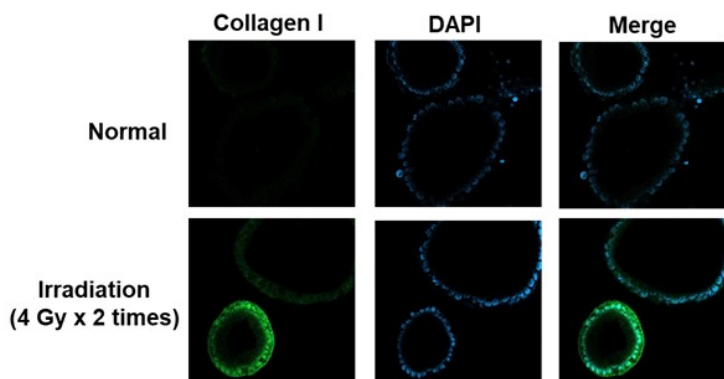
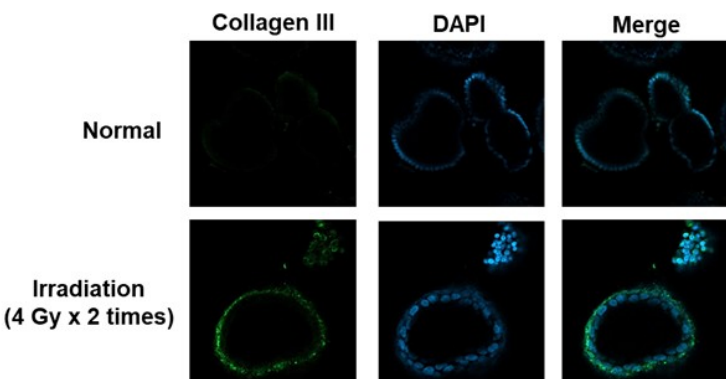
Figure 05**A****B****C****D****E****F****G****H****I****J****K**

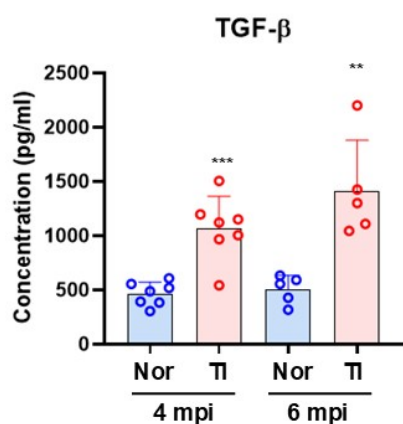
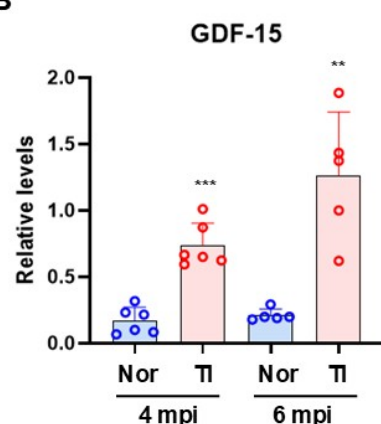
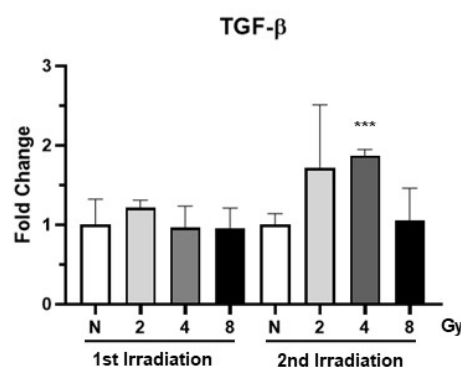
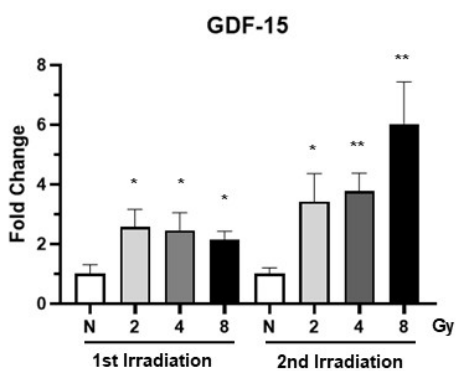
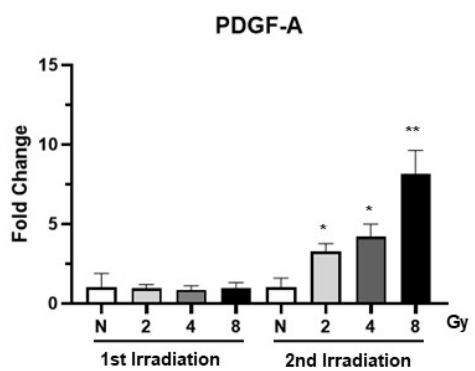
Figure 06**A****B****C****D****E**

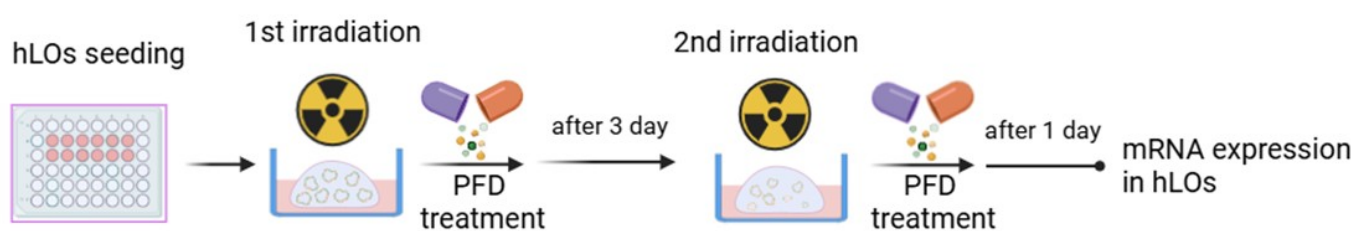
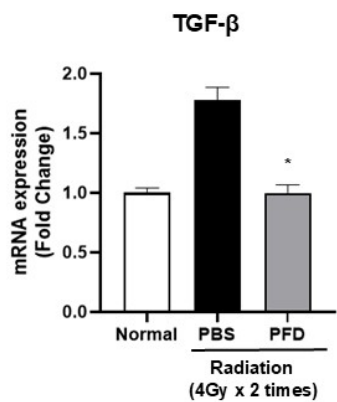
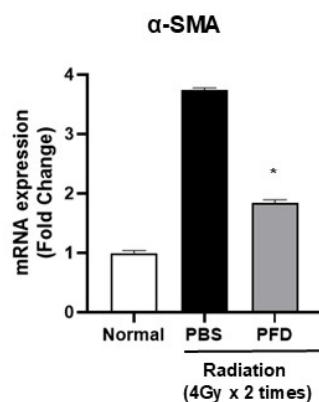
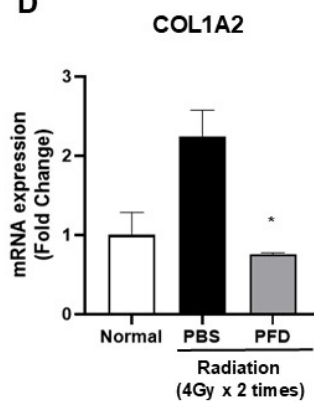
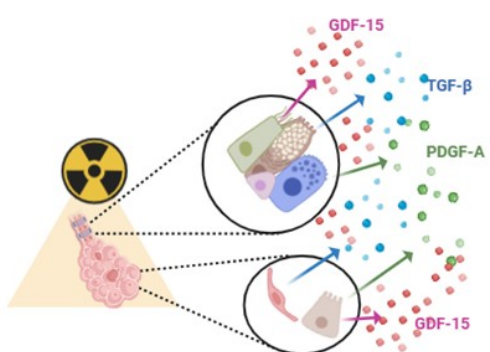
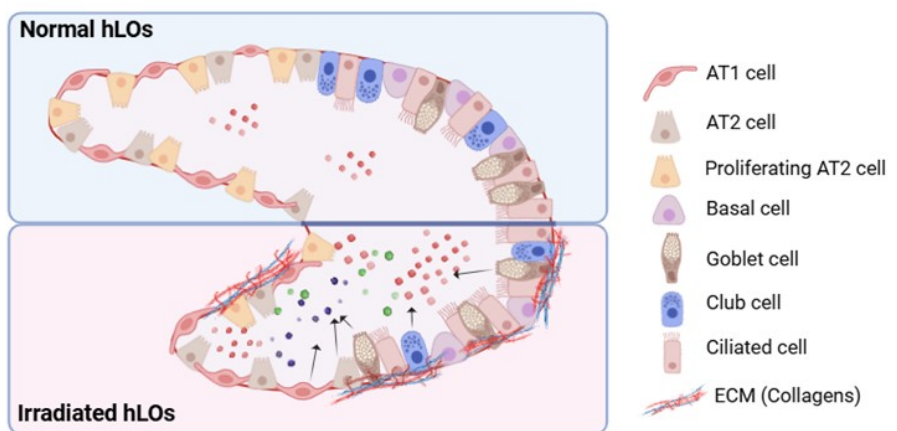
Figure 07**A****B****C****D**

Figure 08**A****B**

Drawing in the Bio-Render app.